Impacts of information flow topology on traffic dynamics of CAV-MV heterogeneous flow

Tiancheng Ruan, Hao Wang, Linjie Zhou, Yantang Zhang, Changyin Dong, Zewen Zuo

***Abstract*—With the development of Connected Autonomous Vehicle (CAV) technology, different information flow topologies (IFTs) have been applied to CAV Ad Hoc Networks. Firstly, from the perspective of the controller, a general model is proposed to directly reflect the actual communication effect on the controller instead of simply abstracting it into the optimal time interval, which is more feasible. Secondly, linear stability analysis is carried out based on the general model where different time delays are considered, and stability criterion is obtained for subsequent analysis. Finally, we compare the three main IFTs through numerical simulations and analyze the difference in stability region, robustness, traffic safety, and Eco-driving between platoon Cooperative Adaptive Cruise Control (CACC) controllers based on different IFTs. It is found that adopting CACCs can notably improve the traffic capacity and traffic safety relative to Manual Vehicle (MV) no matter what IFT is adopted. As for the difference between the three IFTs, predecessor-leader following (PLF) and multiple-predecessor-leader following (MPLF) are significantly superior to predecessor following (PF), while the choice between PLF and MPLF depends on the communication bandwidth. With higher communication bandwidth or fewer communication vehicles, MPLF will be a better option; on the contrary, PLF is more suitable.**

***Index Terms*—Connected and Automated Vehicles (CAVs); CAV platoon; linear stability; platoon management; information topology flow (IFT).**

I. Introduction

WITH the rapid development of transportation systems to optimize traffic safety, mobility, and environmental sustainability, Connected Autonomous Vehicle (CAV) technology has attracted increasing attention and developed rapidly over the past decade. The level of connectivity and automation in vehicles have improved dramatically. Vehicle-to-infrastructure (V2I) communications enable partial or complete autonomous driving with onboard sensors, and vehicle-to-vehicle (V2V) communications enable collaboration and communication between vehicles [1].

The most typical application of V2V communication is Cooperative Adaptive Cruise Control (CACC). A vehicle controlled by this system automatically maintains a constant time gap with the preceding vehicle. Simulation results and field experiments reveal that CACC-enabled vehicles can maintain a shorter time gap than manual vehicles. Therefore, consecutive CACC-enabled vehicles can form a string-based driving mode through V2V communication to improve traffic efficiency [2, 3].

A CAV string consists of a leader vehicle and several following vehicles, maintaining a smaller constant time gap. The formation of CAVs string mainly depends on the workshop communication protocol and the roadside unit communication protocol. The CAV string can break through the limitations of vehicle communication and control and improve traffic efficiency and safety by obtaining more surrounding information in time [4].

Cellular vehicle-to-everything (C-V2X) has been selected as the standard communication protocol for CAVs. However, due to the limitations of C-V2X communication, a CAV string cannot be extended indefinitely, which means that a CAV string is divided into several CAV platoons. The CAV platoon, the subject of this paper, consists of a leader vehicle degraded to Adaptive Cruise Control (ACC) due to loss of communication gain and several CAVs within communication range [5].

At present, there has been much research on CACC string stability. Some studies conducted linear stability analysis of CACC string stability using Partners for Advanced Transportation Technology (PATH)-CACC and Intelligent Driver Model (IDM) as microscopic longitudinal control models [6, 7]. Other studies incorporated assisted strategies for communicating information, such as Connected Cruise Control (CCC), into the framework of linear stability analysis [8, 9].

In general, most current theoretical studies did not precisely reflect the communication function of CACC in the longitudinal control model but calculated the capacity gain brought by it, which is sufficient to simulate the longitudinal behavior of CACC but not suitable for controller design. Furthermore, CACC communication is usually based on Vehicular Mobile Ad Hoc Networks (VANETs), which means communication is based on a specific information flow topology (IFT) in practical application. For the above reasons, the CACC longitudinal control model should also be designed based on a specific IFT, which is ignored by existing research [10, 11, 12].

As for the comparison of the IFTs impact, there are relatively few related studies that mainly focus on comparing the influence of different IFTs on the string stability [13, 14]. In addition, there are many studies on the application of different IFTs in the design of CACC controllers to explore their impact on safety, time headway, and emissions [15, 16, 17]. A systematic and multi-angle study to compare the impacts of

T. Ruan, H. Wang, L. Zhou, C. Dong and Z. Zuo are with the School of Transportation, Southeast University, Nanjing 211189, P.R. China; Jiangsu Key Laboratory of Urban ITS, Southeast University, Nanjing, 210096, P.R. China; Jiangsu Province Collaborative Innovation Center of Modern Urban Traffic Technologies, Southeast University, Nanjing, 210096, P.R. China(e-mail: ruantiancheng@seu.edu.cn; haowang@seu.edu.cn; 220193107@seu.edu.cn; dongcy@seu.edu.cn; 220203312@seu.edu.cn).

Y. Zhang is with School of Transportation Science and Engineering, Harbin Institute of Technology, Harbin, 150090, China(e-mail: 19S132063@stu.hit.edu.cn).

Manuscript received July 1, 2021.(Corresponding author: Hao Wang.)

different IFTs needs to be carried out to help the selection of IFTs.

To fill the gap in this field, this paper takes platoon management and direct information (obtained via communication) into consideration. Firstly, we delivered an extended model considering different IFTs. Secondly, the linear stability analysis was performed to obtain the string stability criterion for the CACC platoon based on the extended model. Finally, the numerical analyses were conducted to determine the difference in stability region, robustness, traffic safety, and Eco-driving of different IFTs. The paper ended with a discussion of analytical results and brief concluding remarks.

The layout of the paper is the following. In Section II, the typical IFTs and the composition of CACC platoon are introduced; In Section III, we propose a general model to simulate CACC longitudinal control and multiple time delays of different vehicles; In Section IV, the linear characteristic equation analytical method is implemented to obtain the string stability criterion of the CACC platoon controller under multiple time delays; In Section V, numerical analyses are used to verify the theoretical analysis results from the perspective of long-wave and short-wave stability, and the differences in stability, robustness, safety, and emission of different IFTs have been explored; In Section VI, main contributions and achievements of this paper are summarized.

II. Analytical expression of heterogeneous traffic flow

A. Typical information flow topologies

The communication module of a CACC system facilitates real-time and reliable wireless V2V/I2V communication, which can not only provide additional information that cannot be readily detected by perception sensors but also more quickly and accurately.

The IFT defines the starting point, terminal point, and the corresponding communication pattern of the CACC, which significantly impacts the effectiveness and efficiency of communication [13]. The three representative IFTs of CACC are shown in Fig. 1. The most commonly used topology is the predecessor following (PF), where the following vehicle only receives the communication signal from its predecessor. However, the inability of PF to obtain information from distant vehicles makes it unable to make full use of the advantages of communication. In response to this feature, predecessor-leader following (PLF) is proposed. Using PLF enables CACC to receive the information from the platoon leader, which means perceiving the traffic conditions far ahead to respond in advance to improve the stability of the traffic flow. The IFT that further leverages the communication ability of CACC is multiple-predecessor-leader following (MPLF) [18, 19]. By utilizing the information of all preceding vehicles in the platoon, the following vehicle can better maintain the stability of the traffic flow. Admittedly, the CACC platoon size cannot be infinite due to the limitation of communication, so platoon management is adopted. The specific measures are to set up rules in the ad-hoc network of CAV that when the platoon size approaches the maximum. While the communication is about to be unstable, the CAV automatically abandons the communication with the platoon leader, degrades to ACC, and forms a new platoon.

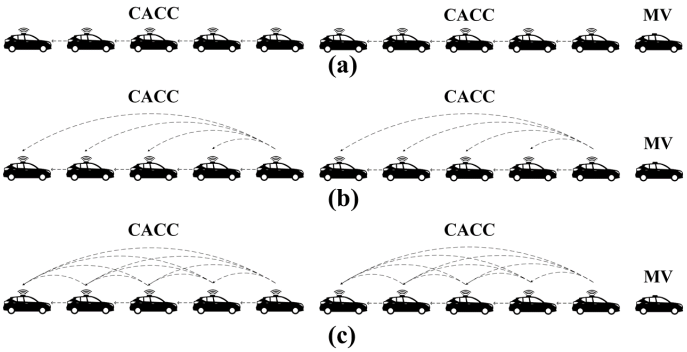

Fig. 1: Typical information flow topologies: (a) predecessor-following (PF), (b) predecessor-leader-following (PLF), (c) multiple-predecessor-leader-following (MPLF).

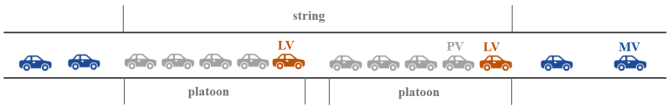

Fig. 2: The Traffic Flow Configurations.

B. Traffic Flow Configurations

As shown in Fig. 2, platoon management is expressed under the condition that when the CACC string reaches the maximum number of vehicles that C-V2X can maintain stable communication, the existing platoon is not included in the subsequent CACC, but a newly-formed platoon. The maximum platoon size S is limited by the maximum C-V2X communication bandwidth. Assume that the traffic flow includes three types of vehicles:

1) *MV* (Manual Vehicle) - regular cars maneuvered by humans;
2) *LV* (Leader Vehicle) - the leader vehicle of the platoon following an MV and its control mechanism is similar to ACC, which cannot obtain the gain of communication and only sends information to its following vehicles [20];
3) *PV* (Platoon Vehicle) - the vehicle inside the platoon which receives information from both preceding vehicle and platoon leader vehicle; The information flow topology of this type of vehicle can be Predecessor-Following (PF), Predecessor-Leader Following (PLF), or multiple-predecessor-leader-following (MPLF) [20].

This paper mainly analyzes the linear string stability of the CACC platoon and designs controllers under different IFTs. The specific platoon consists of a *LV* and $S-1$ *PV*s.

III. Car-Following Model

A. Car-Following Model

In previous studies, there are generally two methods for modeling the car-following behavior of CACCs: 1) simulating

based on modified traffic flow models [21, 22, 23], and 2) modeling based on vehicle models or controllers with experimental data [24, 25, 26]. From the practical application perspective, there is no doubt that the data model based on field tests is closer to the actual situation. However, the high cost and safety risks of CACC field tests make it impractical to conduct large-scale field tests at present. Furthermore, using the fitted model to model the longitudinal behavior abstracts the internal mechanism of the controller, which is not conducive to the design of the CACC controller. In summary, this paper is mainly based on simulations instead of field tests. Moreover, a general form is adopted to simulate longitudinal car-following for the sake of universality and suitability.

1) ACC Model: As for ACC, due to the lack of communication modules, the car-following decision is completely based on its perception of the surrounding situation. According to the existing models used to describe the ACC car-following behavior, its decision-making mainly depends on its velocity, the spacing from the preceding vehicle, and the velocity difference with the preceding vehicle. Therefore, the general form used in this paper is as follows:

$$\frac{dv_n(t)}{dt} = g_n\left(v_n(t-\tau), s_n(t-\tau), \Delta v_n(t-\tau)\right), \tag{1}$$

where $g_n(t)$ is the acceleration; τ is the time delay of decision; $v_n(t)$ is the velocity; $\Delta v_n(t)$ is the velocity difference between the subject vehicle and the preceding vehicle; $s_n(t)$ is the spacing between the subject vehicle and its predecessor.

2) CACC Model: The CACC system, which incorporates a V2V communication module, is an enhancement of the ACC system. With the gain of communication for system stability, CACC can maintain smaller time gaps and perception delays, thereby improving traffic capacity and safety. According to the definition of CACC [27], the essential component is the communication module, which receives information from other CACC-enabled vehicles through VANET. Instead of simply using a smaller time gap to represent communication gain, an additional component has been added to the longitudinal model to describe the communication gain, meaning the information obtained from preceding vehicles via the communication module.

For PF, the transmitted information only includes the position, velocity, and acceleration of the preceding vehicle, so the general form used to simulate CACCs based on PF is as follows:

$$\begin{aligned}\frac{dv_n(t)}{dt} =& g_n\left(v_n(t-\tau), s_n(t-\tau), \Delta v_n(t-\tau)\right) \\ &+ \gamma_p g_{n-1}\left(v_{n-1}(t-\tau), s_{n-1}(t-\tau), \Delta v_{n-1}(t-\tau)\right),\end{aligned} \tag{2}$$

where $g_n(*)$ denotes the acceleration based on the general form of ACC system; γ_p is the weighting coefficient of communication gain from the preceding vehicle.

As for PLF, the transmitted information includes the position, velocity, and acceleration of the platoon leader vehicle and preceding vehicle. In this case, the general form used to simulate CACCs based on PLF is as follows:

$$\begin{aligned}\frac{dv_n(t)}{dt} =& g_n\left(v_n(t-\tau), s_n(t-\tau), \Delta v_n(t-\tau)\right) \\ &+ \gamma_p g_{n-1}\left(v_{n-1}(t-\tau), s_{n-1}(t-\tau), \Delta v_{n-1}(t-\tau)\right) \\ &+ \gamma_l g_1\left(v_1(t-\tau), s_1(t-\tau), \Delta v_1(t-\tau)\right),\end{aligned} \tag{3}$$

where, γ_p is the weighting coefficient of communication gain from preceding vehicle; γ_l is the weighting coefficient of communication gain from leader vehicle.

When the problem comes to MPLF, the transmitted information includes the position, velocity, and acceleration of the platoon leader and all the preceding vehicles in the platoon. Therefore, the expression of the general form for CACC based on MPLF is as follows:

$$\begin{aligned}\frac{dv_n(t)}{dt} =& g_n\left(v_n(t-\tau), s_n(t-\tau), \Delta v_n(t-\tau)\right) \\ &+ \sum_{k=1}^{n-1} \gamma_k g_{n-k}\left(v_{n-k}(t-\tau), s_{n-k}(t-\tau), \Delta v_{n-k}(t-\tau)\right),\end{aligned} \tag{4}$$

where $\gamma_1 = \gamma_2 = \cdots = \gamma_{n-1}$ represent the information communicated from leader and preceding vehicle has identical importance.

B. Perception delays

Different types of vehicles have various reaction delays in the process of obtaining information about the surrounding environment [28, 29]. It is worth noting that reaction delays in this paper refer to the delays of this type. Based on existing research and difference of perceived variables, we can divide the reaction delay into two parts: the reaction delay to the car-following gap τ_n^s, and the reaction delay to the velocity difference $\tau_n^{\Delta v}$, where the reaction delay to vehicle velocity is due to the driver is focusing on the velocity of the vehicle all the time.

1) *MVs*: Since the reaction performance of MVs cannot benefit from the intelligent and connected environment during driving, their time delays do not change. Set the time delay value to: τ_{mv}^s=0.4s, $\tau_{mv}^{\Delta v}$=0.4s;
2) *LVs*: Since LVs are controlled by the Adaptive Cruise Control system, there is no response time delay and decision time delay. However, it cannot communicate, and sensing the state of the vehicle ahead depends entirely on the onboard radar, which has an inevitable sensing delay. Set the delay value to: τ_{lv}^s=0.2s, $\tau_{lv}^{\Delta v}$=0.2s;
3) *PVs*: Due to the intelligent and connected environment, PVs receive the information of the vehicle ahead through the onboard communication system, so its communication delay is almost negligible compared with other delays. Set the delay value to: τ_{pv}^s=0s, $\tau_{pv}^{\Delta v}$=0s.

IV. Linear Stability analysis of CACC platoon controller

In this section, since most of the disturbances faced by drivers during normal driving are tiny disturbances, we apply the linear stability method for the extended intelligent driver model described by Equation (2)-(4) to obtain the stability criterion of the CACC platoon [30, 31]. Since CACCs based

on different IFTs use a similar general model, they can apply the framework of linear stability analysis to obtain the corresponding stability criteria in a similar process. Hence, the following content only takes CACC based on PLF as an example. In the equilibrium state, the vehicle velocity in the traffic flow is equal to the equilibrium state velocity v_e; the velocity difference between adjacent vehicles is zero; the car-following gap between the vehicles maintains the desired gap s_n^e; and the acceleration of the vehicle is zero. So, we can get:

$$\begin{cases} v_n = v_n^e, \\ s_n = s_n^e, \\ \Delta v_n = 0, \\ g_n\left(v_n^e, s_n^e, 0\right) = 0. \end{cases} \tag{5}$$

Now let δv_n and δs_n denote the small deviation of the velocity and gap around the equilibrium state. The state after the disturbance can be expressed as:

$$\begin{cases} v_n = v_n^e + \delta v_n, \\ s_n = s_n^e + \delta s_n, \\ \Delta v_n = 0 + \Delta\left(\delta v_n\right). \end{cases} \tag{6}$$

By introducing the multiple reaction delays into the:

$$\begin{aligned} \frac{d\delta v_n(t)}{dt} &= g_n\left(v_n^e, s_n^e, 0\right) + g_n\left(v_n(t), s_n\left(t-\tau_n^s\right), \Delta v_n\left(t-\tau_n^{\Delta v}\right)\right) \\ &+ \gamma_p g_{n-1}\left(v_{n-1}(t), s_{n-1}\left(t-\tau_{n-1}^s\right), \Delta v_{n-1}\left(t-\tau_{n-1}^{\Delta v}\right)\right) \\ &+ \gamma_l g_1\left(v_1(t), s_1\left(t-\tau_1^s\right), \Delta v_1\left(t-\tau_1^{\Delta v}\right)\right). \end{aligned} \tag{7}$$

Substituting Equation (5) and (6) into (7), the acceleration expression under small disturbance is as follows:

$$\begin{aligned} \frac{d\delta v_n(t)}{dt} =& g_n^v \delta v_n(t) + g_n^s \delta s_n\left(t-\tau_n^s\right) - g_n^{\Delta v}\Delta\left(\delta v_n\left(t-\tau_n^{\Delta v}\right)\right) \\ &+ \gamma_p\left[g_{n-1}^v \delta v_{n-1}(t) + g_{n-1}^s \delta s_{n-1}\left(t-\tau_{n-1}^s\right)\right. \\ &\quad \left. - g_{n-1}^{\Delta v}\Delta\left(\delta v_{n-1}\left(t-\tau_{n-1}^{\Delta v}\right)\right)\right] \\ &+ \gamma_l\left[g_1^v \delta v_1(t) + g_1^s \delta s_1\left(t-\tau_1^s\right) - g_1^{\Delta v}\Delta\left(\delta v_1\left(t-\tau_1^{\Delta v}\right)\right)\right], \end{aligned} \tag{8}$$

$$\frac{d\delta s_n(t)}{dt} = \delta v_{n-1}(t) - \delta v_n(t), \tag{9}$$

where $g_n^v = \left.\frac{\partial g_n}{\partial v_n}\right|_{(v_n^e, s_n^e, 0)}$, $g_n^s = \left.\frac{\partial g_n}{\partial s_n}\right|_{(v_n^e, s_n^e, 0)}$, and $g_n^{\Delta v} = \left.\frac{\partial g_n}{\partial \Delta v_n}\right|_{(v_n^e, s_n^e, 0)}$ are the partial differential equations at the equilibrium state (where the velocity is equilibrium velocity v_n^e, the gap is the equilibrium gap s_n^e and the velocity difference is zero) for velocity, gap, velocity difference, respectively. To obtain the characteristic equation under the disturbance, a reasonable form hypothesis for the disturbance must be proposed. Considering that the disturbance from the preceding vehicle is not equal to zero, the traditional Fourier-ansatz $\delta v_n(t) = \hat{v}e^{\lambda t}$ and $\delta s_n(t) = \hat{s}e^{\lambda t}$ are not applicable. Based on the superposition principle of linear system, Fourier-ansatz can evolve into $\delta v_n(t) = \hat{v}e^{in\varphi+\lambda t}$ and $\delta s_n(t) = \hat{s}e^{in\varphi+\lambda t}$ to represent the disturbance from the preceding vehicle, where $\hat{v}$ and $\hat{s}$ are constants independent of n and t. Based on the Fourier-ansatz and difference equation Equation (9), we can obtain:

$$s_n = \frac{v_{n-1}(t) - v_n(t)}{\lambda}. \tag{10}$$

Take Fourier-ansatz and Equation (10) into (8):

$$\begin{cases} \lambda^2 V_n = \psi_n + \gamma_p \psi_{n-1} e^{-i\varphi} + \gamma_l \psi_1 e^{-i(n-1)\varphi}, \\ \psi_n = \left(g_n^s e^{-\lambda\tau_n^s} - g_n^{\Delta v} e^{-\lambda\tau_n^{\Delta v}}\right)\left(e^{-i\varphi} V_{n-1} - V_n\right) + g_n^v \lambda V_n. \end{cases} \tag{11}$$

The reaction delay term is exponentially expanded to the second order, $e^{-\lambda\tau} = 1 - \lambda\tau + (\lambda\tau)^2/2$, and the third-order characteristic equation of λ is obtained:

$$\begin{aligned} \psi_n =& \left[A_n\lambda^3 + B_n\lambda^2 + C_n\lambda^1 + D_n\lambda^0\right] V_n \\ &+ \left[H_n\lambda^3 + I_n\lambda^2 + J_n\lambda^1 + K_n\lambda^0\right] e^{-i\varphi} V_{n-1}, \end{aligned} \tag{12}$$

where,

$$\begin{cases} A_n = 0.5 g_n^{\Delta v}\left(\tau_n^{\Delta v}\right)^2, \\ B_n = -\left(g_n^{\Delta v}\tau_n^{\Delta v} + 0.5 g_n^s\left(\tau_n^s\right)^2\right), \\ C_n = g_n^v + g_n^{\Delta v} + g_n^s \tau_n^s, \\ D_n = -g_n^s, \\ H_n = -0.5 g_n^{\Delta v}\left(\tau_n^{\Delta v}\right)^2, \\ I_n = g_n^{\Delta v}\tau_n^{\Delta v} + 0.5 g_n^s\left(\tau_n^s\right)^2, \\ J_n = -\left(g_n^{\Delta v} + g_n^s \tau_n^s\right), \\ K_n = g_n^s. \end{cases} \tag{13}$$

Substitute Equation (13) into (11), the third-order characteristic equation of CACC platoon is as follows:

$$\begin{aligned} \lambda^2 V_n =& \left[A_n\lambda^3 + B_n\lambda^2 + C_n\lambda^1 + D_n\lambda^0\right] V_n \\ &+ \left[H_n\lambda^3 + I_n\lambda^2 + J_n\lambda^1 + K_n\lambda^0\right] e^{-i\varphi} V_{n-1} \\ &+ \gamma_p\left[A_{n-1}\lambda^3 + B_{n-1}\lambda^2 + C_{n-1}\lambda^1 + D_{n-1}\lambda^0\right] e^{-i\varphi} V_{n-1} \\ &+ \gamma_p\left[H_{n-1}\lambda^3 + I_{n-1}\lambda^2 + J_{n-1}\lambda^1 + K_{n-1}\lambda^0\right] e^{-i2\varphi} V_{n-2} \\ &+ \gamma_l\left[A_1\lambda^3 + B_1\lambda^2 + C_1\lambda^1 + D_1\lambda^0\right] e^{-i(n-1)\varphi} V_1 \\ &+ \gamma_l\left[H_1\lambda^3 + I_1\lambda^2 + J_1\lambda^1 + K_1\lambda^0\right] e^{-in\varphi} V_0. \end{aligned} \tag{14}$$

To maintain linear string stability of CACC platoons, the solutions of the third-order characteristic equation λ satisfy $\mathrm{Re}(\lambda)\leq 0$. The zero solution $\varphi = 0, \lambda_0 = 0$ of the real number domain that satisfies the conditions can be easily obtained to analyze the changing trend of λ with φ. Suppose λ is the power series solution: Among them, λ_1 and λ_2 are real coefficients. At the same time, expand $e^{-i\varphi N}$ to a second-order power series: $e^{-i\varphi N} = 1 - i\varphi N - \frac{N^2\varphi^2}{2}$. By introducing the periodic traffic scenario and solving the algebraic formula, we can get:

$$\begin{aligned} \Gamma(\varphi) =& \left[C_n + J_n + \gamma_p\left(C_{n-1} + J_{n-1}\right) + \gamma_l\left(C_1 + J_1\right)\right]\lambda_1 \\ &- \left[K_n + \gamma_p\left(D_{n-1} + 2K_{n-1}\right) + \gamma_l\left((n-1)D_1 + nK_1\right)\right] = 0, \end{aligned} \tag{15}$$

$$\begin{aligned} \Gamma\left(\varphi^2\right) =& \left[C_n + J_n + \gamma_p\left(C_{n-1} + J_{n-1}\right) + \gamma_l\left(C_1 + J_1\right)\right]\lambda_2 \\ &- \left[\left(B_n + I_n - 1\right) + \gamma_p\left(B_{n-1} + I_{n-1}\right) + \gamma_l\left(B_1 + I_1\right)\right]\lambda_1^2 \\ &+ \left[J_n + \gamma_p\left(C_{n-1} + 2J_{n-1}\right) + \gamma_l\left((n-1)C_1 + \mathrm{n}J_1\right)\right]\lambda_1 \\ &- \left[0.5K_n + \gamma_p\left(0.5D_{n-1} + 2K_{n-1}\right)\right. \\ &\quad \left. + \gamma_l\left(0.5(n-1)^2 D_1 + 0.5n^2 K_1\right)\right] = 0. \end{aligned} \tag{16}$$

The expression of λ_1 and λ_2 can be obtained by solving the

Equation (15) and (16):

$$\lambda_1 = \frac{\left[K_n + \gamma_p\left(D_{n-1} + 2K_{n-1}\right) + \gamma_l\left((n-1)D_1 + nK_1\right)\right]}{\left[C_n + J_n + \gamma_p\left(C_{n-1} + J_{n-1}\right) + \gamma_l\left(C_1 + J_1\right)\right]} = \frac{g_n^s + \gamma_p g_{n-1}^s + \gamma_l g_1^s}{g_n^v + \gamma_p g_{n-1}^v + \gamma_l g_1^v}, \tag{17}$$

$$\begin{aligned}\lambda_2 = &\frac{\begin{aligned}&\left[(B_n + I_n - 1) + \gamma_p\left(B_{n-1} + I_{n-1}\right) + \gamma_l\left(B_1 + I_1\right)\right]\lambda_1^2 \\ &-\left[J_n + \gamma_p\left(C_{n-1} + 2J_{n-1}\right) + \gamma_l\left((n-1)C_1 + nJ_1\right)\right]\lambda_1 \\ &+\left[0.5K_n + \gamma_p\left(0.5D_{n-1} + 2K_{n-1}\right) + \gamma_l\left(0.5(n-1)^2 D_1 + 0.5n^2 K_1\right)\right]\end{aligned}}{\left[C_n + J_n + \gamma_p\left(C_{n-1} + J_{n-1}\right) + \gamma_l\left(C_1 + J_1\right)\right]} \\ &\begin{aligned}&-\lambda_1^2 + \left[\left(g_n^{\Delta v} + g_n^s\tau_n^s\right) + \gamma_p\left(g_{n-1}^{\Delta v} + g_{n-1}^s\tau_{n-1}^s - g_{n-1}^v\right)\right. \\ &\left.+\gamma_l\left(g_1^{\Delta v} + g_1^s\tau_1^s - (n-1)g_1^v\right)\right]\lambda_1 \\ &+\left[0.5g_n^s + \gamma_p 1.5g_{n-1}^s + 0.5(2n-1)\gamma_1 g_1^s\right] \\ =&\frac{}{g_n^v + \gamma_p g_{n-1}^v + \gamma_l g_1^v}.\end{aligned}\end{aligned} \tag{18}$$

From the conditions of $g_n^s > 0, g_n^v < 0$, it can be known that λ_1 always satisfies the stability condition, then the criterion of string stability becomes $\lambda_2 \le 0$:

$$\begin{aligned}&-\lambda_1^2 + \left[\left(g_n^{\Delta v} + g_n^s\tau_n^s\right) + \gamma_p\left(g_{n-1}^{\Delta v} + g_{n-1}^s\tau_{n-1}^s - g_{n-1}^v\right)\right. \\ &\left.+\gamma_l\left(g_1^{\Delta v} + g_1^s\tau_1^s - (n-1)g_1^v\right)\right]\lambda_1 \\ &+\frac{\left[0.5g_n^s + \gamma_p 1.5g_{n-1}^s + 0.5(2n-1)\gamma_1 g_1^s\right]}{g_n^v + \gamma_p g_{n-1}^v + \gamma_l g_1^v} \le 0.\end{aligned} \tag{19}$$

For the CACC platoon, $g_n^s = g_{n-1}^s = g_1^s$, $g_n^{\Delta v} = g_{n-1}^{\Delta v} = g_1^{\Delta v}$, $g_n^v = g_{n-1}^v = g_1^v$ should be satisfied, which means Equation (19) can be simplified as:

$$\begin{aligned}F_{PLF} &= \left[g_n^{\Delta v}\left(1 + \gamma_p + \gamma_l\right) + g_n^s\left(\tau_n^s + \gamma_p\tau_{n-1}^s + \gamma_l\tau_1^s\right) + \left(\gamma_p + (n-1)\gamma_l\right)g_n^v\right]g_n^v \\ &\quad + (g_n^v)^2\left[0.5 + 1.5\gamma_p + 0.5(2n-1)\gamma_l\right] - g_n^s \\ &= g_n^v g_n^s\left(\tau_n^s + \gamma_p\tau_{n-1}^s + \gamma_l\tau_1^s\right) + g_n^v g_n^{\Delta v}\left(1 + \gamma_p + \gamma_l\right) \\ &\quad + 0.5\left(g_n^v\right)^2\left(1 + \gamma_p + \gamma_l\right) - g_n^s \\ &\ge 0.\end{aligned} \tag{20}$$

For the sake of brevity of the paper, the specific stability criterion derivation process is omitted. Applying the above similar linear stability analysis method, the corresponding string stability criterions of PF and MPLF are as follows:

$$\begin{aligned}F_{PF} = &\, g_n^v g_n^s\left(\tau_n^s + \gamma_p\tau_{n-1}^s\right) + g_n^v g_n^{\Delta v}\left(1 + \gamma_p\right) \\ &+ 0.5\left(g_n^v\right)^2\left(1 + \gamma_p\right) - g_n^s \ge 0,\end{aligned} \tag{21}$$

$$\begin{aligned}F_{MPLF} = &\, g_n^v g_n^s\left(\tau_n^s + \sum_{k=1}^{n-1}\gamma_k\tau_{n-k}^s\right) + g_n^v g_n^{\Delta v}\left(1 + \sum_{k=1}^{n-1}\gamma_k\right) \\ &+ 0.5\left(g_n^v\right)^2\left(1 + \sum_{k=1}^{n-1}\gamma_k\right) - g_n^s \ge 0.\end{aligned} \tag{22}$$

Moreover, based on Equation (20)-(22), a corresponding head-to-tail string stability criterion has also been proposed for three different IFTs [28, 32], since we are comparing the impact of different IFTs applied to CACC platoons. The expression is as follows:

$$\begin{aligned}Q_{PF} = &\left[g_n^v g_n^s\tau_n^s + g_n^v g_n^{\Delta v} + 0.5\left(g_n^v\right)^2 - g_n^s\right] \\ &+ (S-1)\left[g_n^v g_n^s\left(\tau_n^s + \gamma_p\tau_{n-1}^s\right) + g_n^v g_n^{\Delta v}\left(1 + \gamma_p\right)\right. \\ &\left.+0.5\left(g_n^v\right)^2\left(1 + \gamma_p\right) - g_n^s\right] \\ &\ge 0,\end{aligned} \tag{23}$$

$$\begin{aligned}Q_{PLF} = &\left[g_n^v g_n^s\tau_n^s + g_n^v g_n^{\Delta v} + 0.5\left(g_n^v\right)^2 - g_n^s\right] \\ &+ (S-1)\left[g_n^v g_n^s\left(\tau_n^s + \gamma_p\tau_{n-1}^s + \gamma_l\tau_1^s\right) + g_n^v g_n^{\Delta v}\left(1 + \gamma_p + \gamma_l\right)\right. \\ &\left.+0.5\left(g_n^v\right)^2\left(1 + \gamma_p + \gamma_l\right) - g_n^s\right] \\ &\ge 0,\end{aligned} \tag{24}$$

$$\begin{aligned}Q_{MPLF} = &\left[g_n^v g_n^s\tau_n^s + g_n^v g_n^{\Delta v} + 0.5\left(g_n^v\right)^2 - g_n^s\right] \\ &+ \sum_{n=2}^{S}\left[g_n^v g_n^s\left(\tau_n^s + \sum_{k=1}^{n-1}\gamma_k\tau_{n-k}^s\right) + g_n^v g_n^{\Delta v}\left(1 + \sum_{k=1}^{n-1}\gamma_k\right)\right. \\ &\left.+\, 0.5\left(g_n^v\right)^2\left(1 + \sum_{k=1}^{n-1}\gamma_k\right) - g_n^s\right] \\ &\ge 0.\end{aligned} \tag{25}$$

V. Comparisons between different IFTs

In order to explore the differences of different IFTs in stability region, robustness, safety, and emission, several numerical analyses and simulations were adopted in this section. For the stability region, based on the stability criterion of the CACC platoon controller in Equation (20)-(22) obtained in Section IV, numerical analysis on the stability region related to desire time gap and velocity, and a comparison with the traditional ACC controller is conducted. The corresponding simulation verification is carried out under specific parameters. Moreover, we explored the difference of stability region under different controller designs for platoon CACCs, including PF-based, PLF-based, and MPLF-based. As for robustness, safety, and emission, which are difficult to reflect in the numerical analysis. Several related indicators in previous research were proposed to evaluate each aspect of different IFTs. Furthermore, numerical simulations were carried out for each aspect to make comparisons between different IFTs.

To conduct a specific comparative analysis of the differences between different IFTs, a specific model needs to be selected to represent the general form used above. The Intelligent Driver Model (IDM) is chosen for the following reasons. In addition, the general model can be represented by any model that can be used as the ACC control strategy. Firstly, the IDM, having only six parameters with concrete meanings, has been proven to precisely model car-following behaviors. Secondly, many studies used the IDM to model ACC and CACC vehicles [33, 34], which also indicates the ability of the model to reflect operations of driving-assistant systems. The model is expressed as:

$$g_n(t) = A\left[1 - \left(\frac{v_n(t)}{v_f}\right)^{\delta} - \left(\frac{s_0 + T_n v_n(t) + \frac{v_n(t)\Delta v_n(t)}{2\sqrt{Ab}}}{s_n(t) - l_n}\right)^2\right], \tag{26}$$

TABLE I: Parameters chosen for IDM.

Parameter	A	v_f	δ	s_0	b	l
Value	1 m/s^2	33.3 m/s	4	2 m	2 m/s^2	5 m

where $g_n(t)$ is the acceleration; A denotes the maximum desired acceleration; $v_n(t)$ is the velocity; v_f is the free-flow velocity; δ is the acceleration component ($\delta > 0$); s_0 is the minimum safety distance; T_n is the safety time headway; $\Delta v_n(t)$ is the velocity difference between the subject vehicle and the preceding vehicle; b_i is the absolute maximum desired deceleration; $s_n(t)$ is the spacing between the preceding and the subject vehicle; and l_n is the length of the vehicle. The parameters are shown in Table.I [35, 36], which are based on previous studies.

Moreover, the corresponding stability conditions under the IDM can be derived by substituting the partial differential equations of Equation (26): $g^v_{IDM} = -\frac{4Av^3}{v_f^4} - \frac{2AT_n\left[1-(v/v_f)^4\right]}{s^0+vT_n}$, $g^{\Delta v}_{IDM} = \sqrt{\frac{A}{b}}\frac{v\left[1-(v/v_f)^4\right]}{s^0+vT_n}$, and $g^s_{IDM} = 2A\frac{\left[1-(v/v_f)^4\right]^{\frac{3}{2}}}{s^0+vT_n}$ into Equation (23)-(25).

A. Simulation scenario

According to many existing studies [37, 38], using traffic oscillation scenarios to compare the performance of different vehicle types is highly effective. Therefore, we continue to use this method for evaluating the performance of different IFTs on stability region, robustness, safety, and emission. The simulation scenario is as follows:

CACC platoon composition: The simulation platoon includes an MV as the leader vehicle and five CACCs (the maximum platoon size S is assumed to be 5). The CACC following the MV degenerates to ACC, and other vehicles use the car-following model with general form as the longitudinal control model.

Simulation scheme: At first, all vehicles maintain the same initial velocity and the desire time gap. In order to simulate most traffic scenarios, the disturbance is applied to the leader vehicle. Besides, the most common three disturbances are adopted, including:

1) *Type I Sine disturbance*: The acceleration of leader vehicle MV shows a sine wave with a period of 9s and a magnitude of 0.16 m/s^2 in 5s−41s.
2) *Type II Custom disturbance*: The leader vehicle suddenly accelerates to 11.8m/s in 5s and keeps the velocity for 15s. The leader vehicle then decelerates to 8.2m/s and accelerates to 10m/s, while the following vehicles respond to this traffic oscillation scenario.
3) *Type III Impulse disturbance*: The form of disturbance is that the acceleration of the leader vehicle suddenly rose to 0.9 m/s^2 and -0.9 m/s^2 at 4s and 40s, respectively.

The specific speed and acceleration curve figures of the leader vehicle under different disturbances are shown in Fig. 3. Moreover, each simulation for evaluating indicators is conducted ten times to avoid random error.

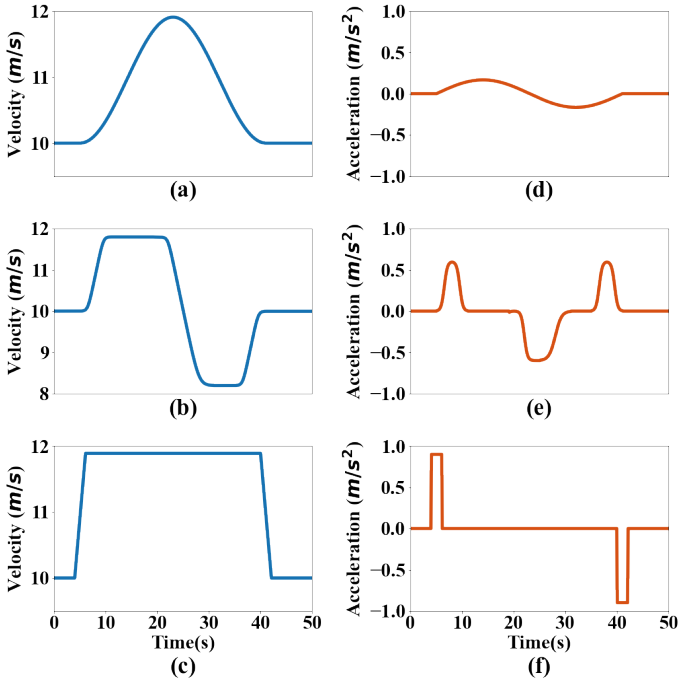

Fig. 3: The specific speed and acceleration curve figures of the leader vehicle under different disturbances. (a)-(c) the speed curve of Type I, Type II, and Type III; (d)-(f) the acceleration curve of Type I, Type II, and Type III

B. Comparison of stability region

As an essential basis for the design of a controller, string stability must be ensured to avoid the disturbance from the upstream being amplified in the downstream traffic flow. So, the first item of comparison is the stability region of different IFTs.

1) Margin stable curves of different IFTs: The basic principle of controller design is that a controller can keep string stable, so it is necessary to compare the margin stable curves of the three IFTs that can keep the string stable to get the margin stable time gap directly related to the traffic capacity.

Assuming the information from the leader and preceding vehicle is of equal importance, the γ_p is set equal to γ_l in this study. In addition, the weighting coefficient of communication gain of different IFTs is set to 0.3 to make them comparable. Based on the head-to-tail string stability criterion of different IFTs in Equation (23)-(25), the heatmaps in the control space (velocity-desire time gap) are expressed in Fig. 4, and the black curve in each subfigure represents the margin stable curve. When the traffic flow environment and desire time gap setting is above the margin stable curve, it is string stable at equilibrium state, while the opposite represents the unstable traffic flow.

Firstly, we focused on the head-to-tail string stability of different IFTs in the control space (velocity-desire time gap). It can be quickly noticed that there is a significant unstable peak in the cases of PF, ACC, and MV. Furthermore, this peak means that the head-to-tail string stability deteriorates over a specific velocity interval, adversely affecting traffic flow. Moreover, the head-to-tail string stability is sensitive to the

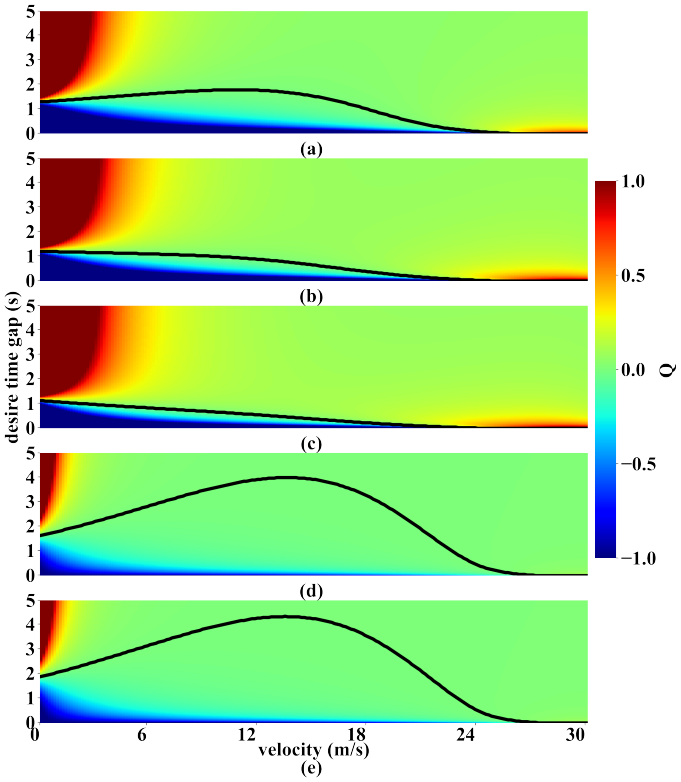

Fig. 4: The heatmaps in the velocity-desire time gap of different IFTs. (a) the case of PF; (b) the case of PLF; (c) the case of MPLF; (d) the case of ACC; (e) the case of MV.

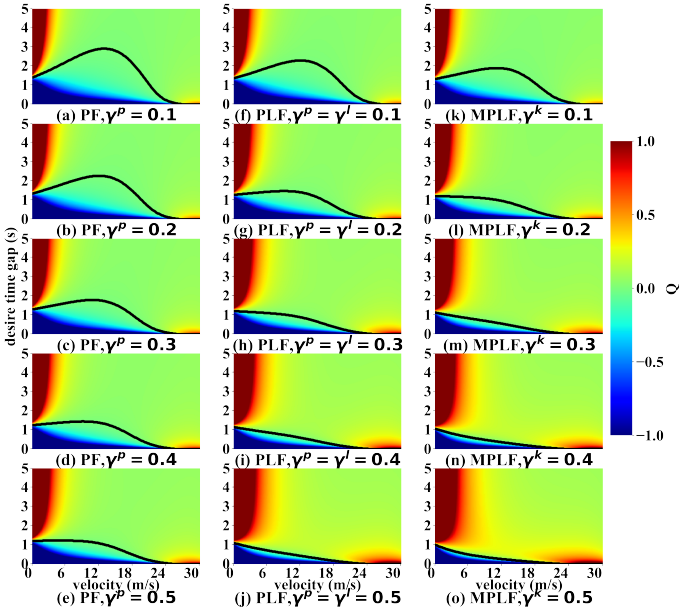

Fig. 5: The heatmaps in the velocity-desire time gap of different IFTs under different parameters setting. (a)-(e) the case of PF; (f)-(j) the case of PLF; (k)-(o) the case of MPLF.

desire time gap under low velocity but is insensitive under high velocity. In addition, all subfigures show the tendency that the margin stable curve is close to 0s under high velocity, which may be due to head-to-tail string stability being easier to maintain when the velocity is increased. From another perspective, both the heatmaps and margin stable curves of ACC and MV are similar, which is consistent with the conclusions reached in other studies.

Secondly, the difference between (a), (b), and (c) is worth noticing. It can be seen from Fig. 4 that the margin stable curves of ACC and IDM are of distinct orders of magnitude compared with those of PF, PLF, and MPLF under different parameter settings, which means the adoption of CACC can significantly improve the traffic capacity by reducing desire time gap. For the CACC platoon controllers, it can be found that the margin stable curves are significantly lower than the ACC curve and are lower as parameters increase, which means obtaining the information from the preceding vehicle via communication can significantly improve the long-wave stability of traffic flow. Moreover, the curve of PF has a significantly unstable peak which is similar to the curves of ACC and MV. In contrast, the curves of PLF and MPLF can efficiently suppress the appearance of this peak under similar parameter settings to maintain a lower desire time gap in the entire velocity range. In addition, the curve of PLF is significantly lower than the curve of PF, and the critical desire time gap is only 39.53% of PF when velocity = $10m/s$. This indicates that the controller based on PLF and MPLF can significantly improve traffic flow stability compared with PF on enhancing traffic flow capacity and safety. As for the difference between the margin stable curves of PLF and MPLF, the curve of MPLF is lower than the curve of PLF, and the reduced proportion is 41.18% when velocity = $10m/s$, which means that obtaining more information from the further preceding vehicles can improve the stability of traffic flow. However, the reduced proportion of MPLF in the entire velocity range is only 30.41%.

Based on the above analysis, one conclusion can be drawn that MPLF can keep the desire time gap to a minimum without losing head-to-tailing stability among IFTs. Both PLF and MPLF are able to suppress deterioration of stability due to increased velocity, whereas PF is not.

2) Margin stable curves of IFTs under different parameters: In Section V-B1, the weighting coefficient of communication gain of different IFTs is all set to 0.3 to make them comparable. However, another problem arises with setting the weighting coefficient of communication gain. For this purpose, the numerical analysis of the different parameter settings is also carried out. Derived from Equation (23)-(25), the heatmaps in the control space (velocity-desire time gap) under different parameter settings are expressed in Fig. 5, and the black curve in each subfigure represents the margin stable curve.

It can be clearly found in Fig. 5, margin stable curves of all IFTs decline as parameters setting increases, which means that an appropriate increase in weighting coefficient of communication gain can help reduce desire time gap without losing head-to-tail string stability. From another perspective, the curve of all IFTs with lower parameter settings will have a significant peak as the velocity increases. However, as for PF, this peak is not disappeared even if the parameter

is set to 0.5, while the PLF and MPLF only need 0.3 to suppress. As for the differences between different parameters, the curves show a trend of getting closer with the parameters increasing. Moreover, the control of the vehicle will tend to follow the control strategy of the preceding vehicle rather than use its own, which means that the controller relies more on communication. However, the communication environment is not reliable enough to make decisions only based on the information communicated yet since the illegal channel occupation and obstacle interference are everywhere. For the reasons above, a more significant parameter value is not necessary to improve string stability, so we choose $\gamma_p = \gamma_l = \gamma_k = 0.3$ in the following simulations.

3) Simulation validation of theoretical results: To verify the results of theoretical numerical analysis from the perspective of short-wave stability of traffic flow, the stability region validation is conducted in the disturbance *Type I*.

stability region validation: To validate the stability region of different IFTs obtained in Section V-B1, simulations under traffic settings with different values of desire time gap and velocity are conducted. Here we divided the velocity range $(0-30m/s^2)$ by an interval of $0.3m/s^2$ where a break of 0.02s separated the desire time gap (0-2s). Note that the validation of the stability region is only conducted at 0-2s desire time gap since the margin curves of three IFTs are lower than 2s at the entire velocity range, and only disturbance *Type I* is adopted to avoid too much computational burden. The stability region obtained by simulations is shown in Fig. 6, where the black curve shows the margin stable curve in the theoretical results, and the blue region depicts the stability region in simulation while the orange region depicts the instability region.

From Fig. 6, one conclusion that can be drawn is that the simulation results and theoretical results remain highly consistent since the margin stable curve almost coincides with the dividing line on the heatmaps. In addition, it is easier to ensure string stability that the desire time gap increases, both in theoretical and simulation results. It is important to note that when the velocity is in the interval close to 0 m/s, the desire time gap corresponding to the margin stable in the simulation result is lower than the margin stable curve. One reason for speculation is that the disturbance *Type I* we applied is a pure acceleration disturbance causing its actual average velocity to deviate from 0 m/s as the equilibrium velocity and is quite different from the equilibrium velocity. In general, the above results show that the theoretical results of linear stability analysis agree with those of the simulation of short-wave stability.

C. Comparison of robustness

In practical application, channel occupancy and the obstacle within the communication range make the communication environment not absolutely ideal, making it necessary to ensure the robustness of the corresponding IFTs. Notice that the unreliable communication environment mentioned here refers to interference on the effect of communication, and cyber-attacks are not considered since the corresponding network security strategy should be activated. There are many indicators that

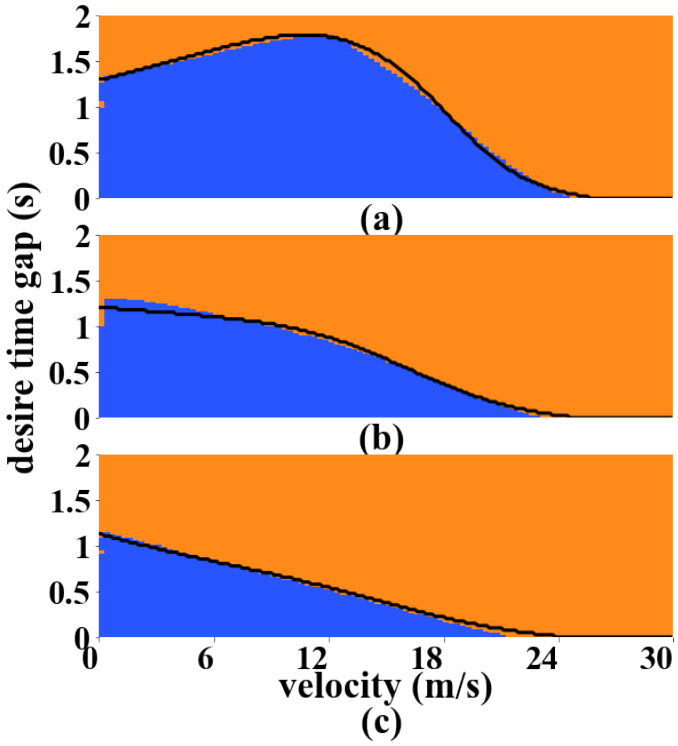

Fig. 6: The heatmaps of simulation results in the velocity-desire time gap under different IFTs. (a) the case of PF; (b) the case of PLF; (c) the case of MPLF.

characterize unreliable communication environments, such as Channel Busy Ratio (CBR), delay, Packet Error Ratio (PER), and Inter-Transmit Time (ITT). As for CBR and ITT, the effect on communication is reflected in PER. According to the report on the fourteenth meeting of IMT-2020 (5G) Promotion Group Cellular-Vehicle-to-everything Working Group, delays remain stable and below 61.5ms with 110 On-Board Units (OBUs) within a 100m radius. Therefore, PER is selected as the indicator to represent the unreliable communication environment. To verify the robustness of different IFTs, we simulated the CACC platoon equipped with different IFTs in a non-ideal communication environment with several PER (5%, 10%, 20%) and 10Hz communication frequencies. Here we divided the velocity range $(0-30m/s)$ by an interval of $0.75m/s$ where a break of 0.05s separated desire time gap (0-2s). IFT parameter settings similar to those in Section V-A are adopted in the simulation, with three types of disturbances applied. In addition, to quantify the effects of unreliable communication, we choose the PER of 0% as the benchmark for comparison and the absolute value of the velocity difference as the indicator to represent the impact, which a higher value indicates a larger impact. The simulation results are shown in Fig. 7, Fig. 8, and Fig. 9.

First of all, the influence of equivalent PERs on different IFTs is analyzed. We can sum up from Fig. 7 - 9 that PER has the minor impact on PF, while MPLF has the biggest. At a PER of 20%, PFs can maintain the same state as the one with ideal communication in most of the control space. On the contrary, PLF and MPLF have noteworthy differences. This

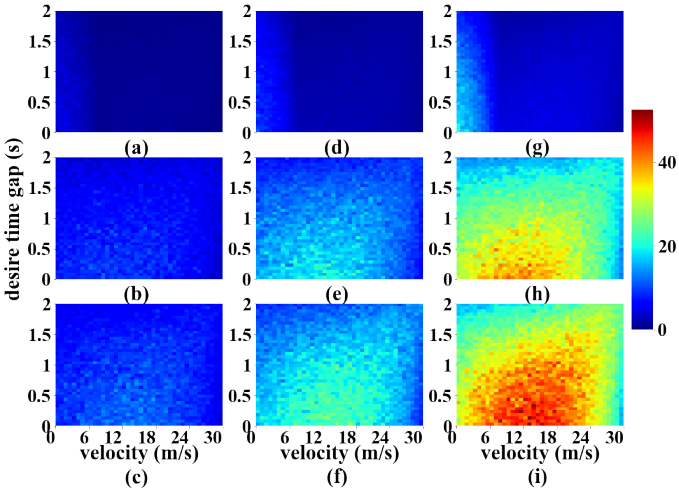

Fig. 7: The heatmaps of the velocity difference against ideal communication among three IFTs with different PER under disturbance *Type I*. (a)-(c) the case with 5% PER; (d)-(f) the case with 10% PER; (g)-(i) the case with 20% PER. (a),(d),(g) The case of PF; (b),(e),(h) The case of PLF; (c),(f),(i) The case of MPLF.

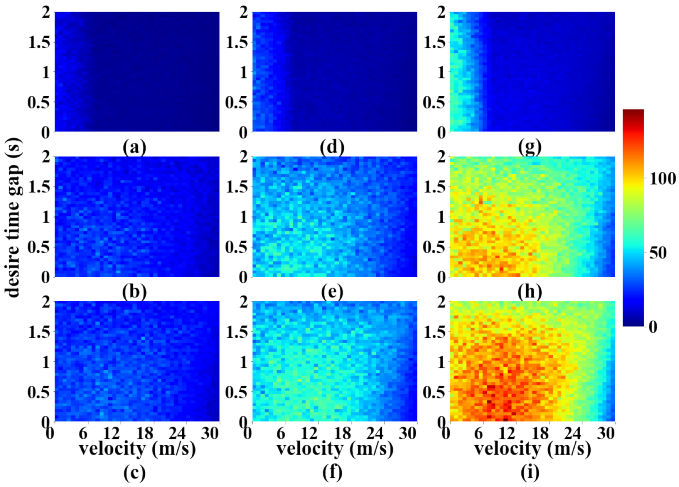

Fig. 8: The heatmaps of the velocity difference against ideal communication among three IFTs with different PER under disturbance *Type II*. (a)-(c) the case with 5% PER; (d)-(f) the case with 10% PER; (g)-(i) the case with 20% PER. (a),(d),(g) The case of PF; (b),(e),(h) The case of PLF; (c),(f),(i) The case of MPLF.

phenomenon is quite understandable because more communication demand leads to more communication failures under the same PERs, which further seriously impacts car-following behaviors. As for the influence of different PERs, a reasonable conclusion can be drawn that its impact greatly increases with the rise of PER. Considering the impact of different disturbance types, we can find that *Type II* has far more impact than *Type I* and *Type III*. The phenomenon can be interpreted that *Type II* has the greatest scale of duration and magnitude than the other two, which brings the most significant advantage with ideal communication. However, this advantage will be

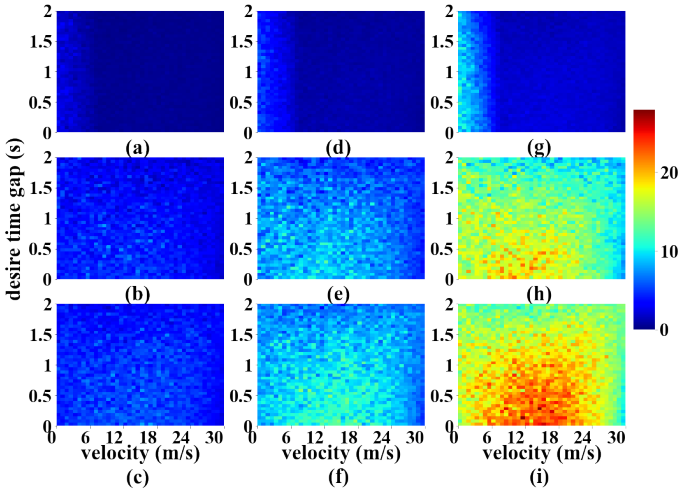

Fig. 9: The heatmaps of the velocity difference against ideal communication among three IFTs with different PER under disturbance *Type III*. (a)-(c) the case with 5% PER; (d)-(f) the case with 10% PER; (g)-(i) the case with 20% PER. (a),(d),(g) The case of PF; (b),(e),(h) The case of PLF; (c),(f),(i) The case of MPLF.

weakened when the communication is unreliable. Moreover, the larger the weakening, the bigger the influence.

As for the specific impact of PER, we have selected the case with velocity at $10m/s$, PER at 20%, and desire time gap at $1.2s$ as an example for analysis, the curves of velocities and accelerations are shown in Fig. 10.

PER appears as a sudden increase or decrease of the acceleration in Fig. 10. Admittedly, poor communication quality can significantly affect the stability of the CACC platoon, especially in continuous packet error. However, due to high communication frequency, the velocity curves of PF and PLF remain steady. At the same time, few disturbances on accelerations show that platoon controllers designed based on PF and PLF are robust against such communication failures. They can still guarantee smooth driving even under poor communication quality. On the other hand, platoon controllers designed based on MPLF are not robust against such communication failures and cannot maintain an appropriate time gap due to their dependence on ideal communication. Moreover, more communication requirements are needed for MPLF to achieve a smaller desire time gap, but the reduction in the desire time gap will bring a surge in communication requirements that is difficult to achieve. According to corresponding research [39], the failure rate of communication is 16% when the communication frequency is 2 packet/s, and when the communication frequency is 5 packet/s, the failure rate is 38%. This indicates that as the communication demand in the same channel approaches the channel bandwidth, the communication failures will significantly increase. Therefore, the gain on the margin stable curve and its negative impact on communication instability should be considered balanced. To summarize, PF and PLF are more suitable IFTs in terms of robustness.

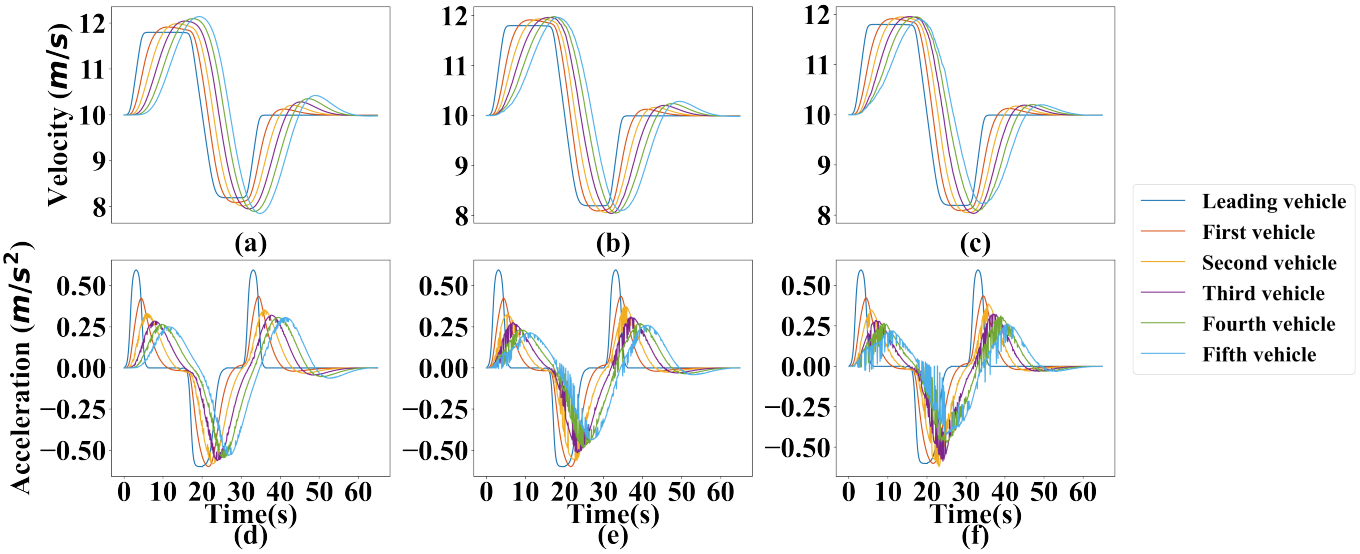

Fig. 10: Time evolutions of the velocity and acceleration of simulation platoon for different IFTs with the velocity at $10m/s$, PER at 20%, and desire time gap at $1.2s$. (a)-(c) the subplots of the velocity curves; (d)-(f) the subplots of the velocity curves; (a),(d) the case of PF; (b),(e) the case of PLF; (c),(f) the case of MPLF.

D. Comparison of traffic safety

In addition to stability, safety is another essential reference factor for controller design. Two indicators, such as Maximum Time To Collision (MTTC) and Deceleration Rate to Avoid the Crash (DRAC), are selected to compare the security performance of platoon controllers based on different IFTs. The corresponding indicators are calculated as follows:

$$MTTC_t = \frac{v_{F,t} - v_{L,t} \pm \sqrt{(v_{F,t} - v_{L,t})^2 + 2\Delta a_t \left(x_{L,t} - x_{F,t} - D_L\right)}}{\Delta a_t}, \tag{27}$$

$$DRAC_{F,t} = \frac{(v_{F,t} - v_{L,t})^2}{2\left(x_{L,t} - x_{F,t} - D_L\right)}, \tag{28}$$

where $x_{L,t}$ and $x_{F,t}$ denotes the positions of the leading vehicle and the following vehicle at time t, respectively; $v_{F,t}$ and $v_{L,t}$ are their velocities at time t; D_L is the length of the leading vehicle; Δa_t is the relative acceleration of conflicting vehicles at time t; $t_{F,t}$ and $t_{L,t}$ are the time of following vehicle arrives and leading vehicle leaves encroachment time. Simulation is implemented based on similar IFT parameter settings in Section V-A, and all disturbance types are adopted in simulation. Fig. 11 and Fig. 12 show the heatmap of different IFTs compared with pure MV environment as the baseline on various indicators under three disturbances in the control space (velocity-desire time gap). It should be noted that the MTTC is the larger, the safer, while the DRAC is the smaller, the safer. Therefore, the improvement rate mentioned here refers to the increased proportion of IFT compared to MV for MTTC, representing the reduced proportion for DRAC. Moreover, the black curve in each subfigure represents the margin stable curve of the corresponding IFT.

First, we focus on the distribution of heatmaps in each subplot. No matter what kind of disturbances and what kind of IFTs, heatmaps all show a trend that the increased proportion

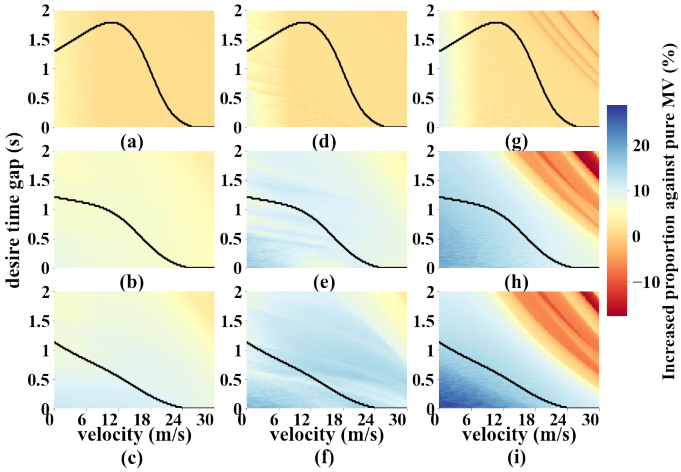

Fig. 11: Increased proportion heatmaps of MTTC among three IFTs against pure MV under three disturbances. (a)-(c) the case under disturbance *Type I*; (d)-(f) the case under disturbance *Type II*; (g)-(i) the case under disturbance *Type III*. (a),(d),(g) The case of PF; (b),(e),(h) The case of PLF; (c),(f),(i) The case of MPLF.

decreases as the velocity and desire time gap increase in the control space (velocity-desire time gap). Notices that for DRAC, all IFTs are able to maintain better safety conditions against MVs, while some areas are not as good as MVs for MTTC, which may be due to significantly increased string stability of MVs at the high desire time gap and velocity.

The second thing to note is the difference in heatmaps between different IFTs under the same disturbance. From Fig. 11 and 12, a phenomenon can find that IFTs with more communication information can maintain better safety conditions that are significantly larger than the case of PF when velocity and desire time gap is low. However, from the

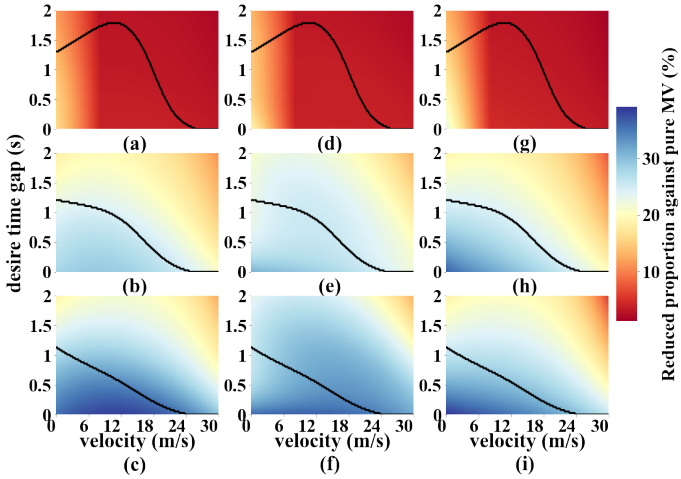

Fig. 12: Reduced proportion heatmaps of DRAC among three IFTs against pure MV under three disturbances. (a)-(c) the case under disturbance *Type I*; (d)-(f) the case under disturbance *Type II*; (g)-(i) the case under disturbance *Type III*. (a),(d),(g) The case of PF; (b),(e),(h) The case of PLF; (c),(f),(i) The case of MPLF.

point of view of the whole control space, IFTs with more communication information are greatly affected by the change of velocity and desire time gap, while PF has little difference.

As for the differences between different disturbances in the same IFT, most groups of subplots in Fig. 11 and Fig. 12 show that the degree of impact on MTTC gradually increases from *Type I* to *Type III*. This phenomenon is easy to understand because the three disturbances change more and more dramatically on the acceleration, which is not conducive to traffic safety. However, the law above does not apply to DRAC for MPLF. Better safety conditions can be provided under disturbance *Type I* than under the *Type II* or *Type III* disturbance for MPLF.

Given the above, using PLF and MPLF can improve traffic safety compared to MV and PF in most scenarios. In addition, having more communication information helps maintain better security conditions at low velocity but worsens at high velocity. PLF and MPLF are therefore more inclined to adopt than PF from the point of view of traffic safety.

E. Comparison of Eco-driving

With the substantial increase in the number of vehicles, CACCs are also considered a solution, so it is necessary to incorporate pollutant emissions into comparing different IFTs. Panis et al. [40] established an emission model using a nonlinear multivariate regression based on field measurement. The expression for calculation instantaneous traffic emission of a specific vehicle is:

$$E_i(t) = \max\left[0, f_1 + f_2 v_i(t) + f_3 v_i(t)^2 + f_4 a_i(t) + f_5 a_i(t)^2 + f_6 v_i(t) a_i(t)\right], \tag{29}$$

where $E_i(t)$ is the pollutant emission for the vehicle in unit time (g/s); f_1 to f_6 are emission parameters for each type of pollutant; $v_i(t)$ is the velocity of the subject vehicle; and $a_i(t)$ is the acceleration of the subject vehicle. Values of emission parameters are provided in Table.II. The simulation scenario

TABLE II: Parameters for Emission Model of Petrol Car.

Pollutant		f_1	f_2	f_3	f_4	f_5	f_6
CO_2		5.53e-01	1.61e-01	-2.89e-03	2.66e-01	5.11e-01	1.83e-01
NO_x	$a \geq -0.5$ m/s^2	6.19e-04	8.00e-05	-4.03e-06	-4.13e-04	3.80e-04	1.77e-04
	$a < -0.5$ m/s^2	2.17 e-04	0	0	0	0	0
VOC	$a \geq -0.5$ m/s^2	4.47e-03	7.32e-07	-2.87e-08	-3.41e-06	4.94e-06	1.66e-06
	$a < -0.5$ m/s^2	2.63e-03	0	0	0	0	0

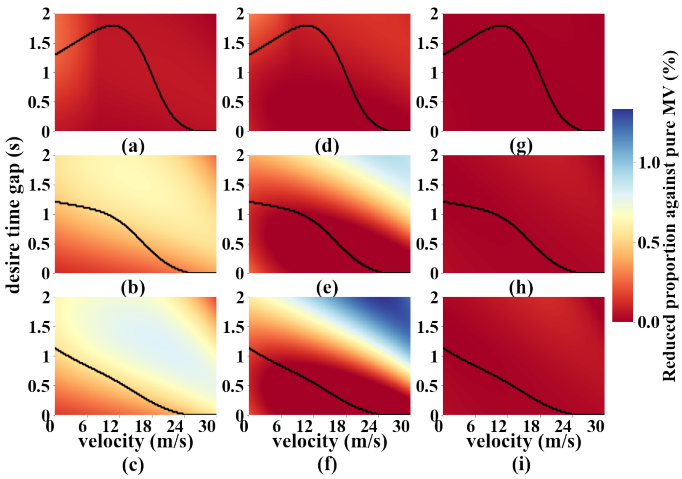

Fig. 13: Reduced proportion heatmaps of CO_2 among three IFTs against pure MV under three disturbances. (a)-(c) the case under disturbance *Type I*; (d)-(f) the case under disturbance *Type II*; (g)-(i) the case under disturbance *Type III*. (a),(d),(g) The case of PF; (b),(e),(h) The case of PLF; (c),(f),(i) The case of MPLF.

is the same as Section V-A with all three disturbances. The heatmaps of different IFTs under three disturbance types with pure MV setting as the baseline on three pollutant emissions are shown in Fig. 13, Fig. 14, and Fig. 15 with a black curve in each subplot representing the margin stable curve of the corresponding IFT.

Heatmaps demonstrate that the adoption of IFTs does reduce pollution emissions against pure MV, and the magnitude of emission reduction of different emissions are also different. As for VOC and CO2, the reduced proportion is less than 1.5% in the whole control space under three types. For NOx, by contrast, the effect is significant as the reduced proportion is up to 7.8% under disturbance *Type II*.

From the perspective of the distribution of heatmaps in each subplot, Fig. 13 and Fig. 14 illustrate that the reduced proportion increases with the desire time gap and velocity for NOx and CO2. As for heatmaps in Fig. 15, a different phenomenon is that the region can maintain lower emissions in the middle of control space, and the range of the area becomes smaller as the velocity increases.

From the perspective of differences between different disturbances, all pollutants show that IFTs can reduce pollutant emissions against pure MV under disturbance *Type I* and disturbance *Type II*, while is the same as MV under disturbance *Type III*. Moreover, under disturbance *Type II*, IFTs have the most significant impact on reducing pollutant emissions. From

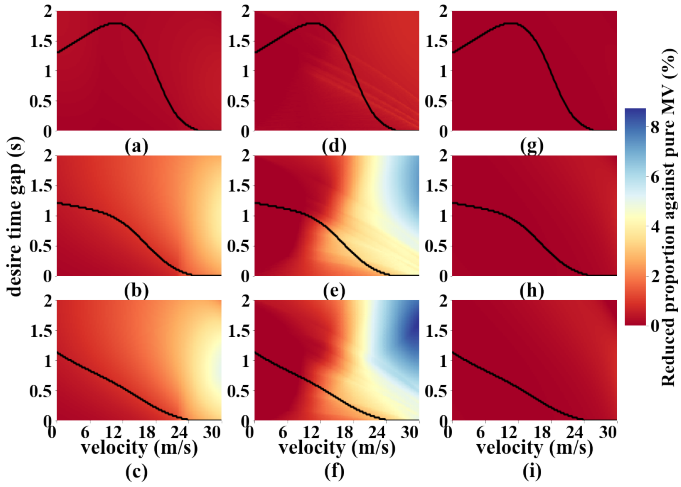

Fig. 14: Reduced proportion heatmaps of NO_x among three IFTs against pure MV under three disturbances. (a)-(c) the case under disturbance *Type I*; (d)-(f) the case under disturbance *Type II*; (g)-(i) the case under disturbance *Type III*. (a),(d),(g) The case of PF; (b),(e),(h) The case of PLF; (c),(f),(i) The case of MPLF.

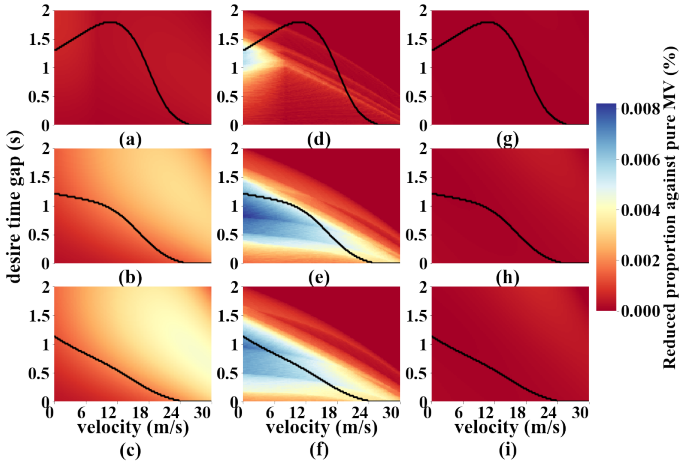

Fig. 15: Reduced proportion heatmaps of VOC among three IFTs against pure MV under three disturbances. (a)-(c) the case under disturbance *Type I*; (d)-(f) the case under disturbance *Type II*; (g)-(i) the case under disturbance *Type III*. (a),(d),(g) The case of PF; (b),(e),(h) The case of PLF; (c),(f),(i) The case of MPLF.

another perspective, adopting PF does not cause noteworthy differences compared to pure MV, while adopting PLF and MPLF can.

To summarize, although IFTs can only significantly reduce partial pollution emissions in the case of some types of disturbances, PLF and MPLF can substantially be superior to PF from the Eco-driving perspective in the three IFTs comparisons.

F. Impact of actuation delay

The actuation delay is another inevitable nature property of the actuators and sensors in the mechanical and control systems. According to relevant research, the stability analysis is also affected by the actuation delay as well as perception delays discussed before [41, 42, 43]. Therefore, the string stability analyses of different IFTs considering the actuation delay are conducted in this paper. It should be clarified that the derivation of the stability conditions considering the actuation delay is also based on the PLF for simplicity.

By considering the actuation delay, the general form of PLF-abled CACCs is as follows:

$$\begin{aligned}\frac{dv_n(t)}{dt} = & g_n\left(v_n(t-\tau^*), s_n(t-\tau^*), \Delta v_n(t-\tau^*)\right)\\ & +\gamma_p g_{n-1}\left(v_{n-1}(t-\tau^*), s_{n-1}(t-\tau^*), \Delta v_{n-1}(t-\tau^*)\right)\\ & +\gamma_l g_1\left(v_1(t-\tau^*), s_1(t-\tau^*), \Delta v_1(t-\tau^*)\right),\end{aligned} \tag{30}$$

where $\tau^* = \tau+\eta$ denotes the full delay, including the perception delay and the actuation delay, η represents the actuation delay.

By introducing the small deviation of the velocity around the equilibrium state and the multiple reaction delays into Equation (30):

$$\begin{aligned}\frac{d\delta v_n(t)}{dt} = & g_n\left(v_n^e, s_n^e, 0\right) + g_n\left(v_n(t-\tau_n^{v^*}), s_n\left(t-\tau_n^{s^*}\right), \Delta v_n\left(t-\tau_n^{\Delta v^*}\right)\right)\\ & +\gamma_p g_{n-1}\left(v_{n-1}(t-\tau_{n-1}^{v^*}), s_{n-1}\left(t-\tau_{n-1}^{v^*}\right), \Delta v_{n-1}\left(t-\tau_{n-1}^{\Delta v^*}\right)\right)\\ & +\gamma_l g_1\left(v_1(t-\tau_1^{v^*}), s_1\left(t-\tau_1^{v}\right), \Delta v_1\left(t-\tau_1^{\Delta v^*}\right)\right),\end{aligned} \tag{31}$$

where $\tau_n^{v^*} = \eta$, $\tau_n^{s^*} = \tau_n^s+\eta$, and $\tau_n^{\Delta v^*} = \tau_n^{\Delta v}+\eta$ represents the full delay of the velocity, gap, and velocity difference, respectively.

What needs to be mentioned is that Equation (15) and Equation (16) need to be extended to three-order to derive the corresponding conclusions in order to explore the impact of the actuation delay.

Adopting string stability analyses in Equation (8)-Equation (20), the stability conditions considering both the perception delays and the actuation delay are as follows:

$$\begin{aligned}F_{PLF}^* = & -(g_n^v)^2 g_n^{\Delta v}\phi_1{}^2 + (g_n^v)^3\phi_1\phi_2 + (g_n^v)^2 g_n^s\phi_1\phi_3 - g_n^v\left(g_n^{\Delta v}\right)^2\phi_1{}^2\\ & -g_n^v g_n^{\Delta v} g_n^s\phi_1\left(2\phi_4-\phi_5\right) - g_n^v(g_n^s)^2\left(\phi_4{}^2 + \tfrac{1}{2}\phi_1\phi_6 - \tfrac{1}{2}\phi_1\phi_8\right)\\ & -g_n^v g_n^s\left(\phi_7 + \tfrac{1}{2}\phi_1\right) + (g_n^v)^{-1}(g_n^s)^2 \geq 0,\end{aligned} \tag{32}$$

where,

$$\begin{cases}\phi_1 = \left(1+\gamma_p+\gamma_l\right)\\ \phi_2 = (\gamma_p + \frac{n(n-1)}{2}\gamma_l)\\ \phi_3 = \left(-\frac{1}{2}\tau_n^{v^*} - \frac{1}{6}\right) + \gamma_p\left(\frac{1}{2}\tau_{n-1}^{v^*} - \frac{7}{6}\right) + \gamma_l\left(\frac{2n-3}{2}\tau_1^{v^*} - \frac{3n^2-3n+1}{6}\right)\\ \phi_4 = \tau_n^{s^*} - \tau_n^{v^*} + \gamma_p\left(\tau_{n-1}^{s^*} - \tau_{n-1}^{v^*}\right) + \gamma_l\left(\tau_1^{s^*} - \tau_1^{v^*}\right)\\ \phi_5 = \tau_n^{\Delta v^*} + \gamma_p\tau_{n-1}^{\Delta v^*} + \gamma_l\tau_1^{\Delta v^*}\\ \phi_6 = \left(\tau_n^{s^*}\right)^2 + \gamma_p\left(\tau_{n-1}^{s^*}\right)^2 + \gamma_l\left(\tau_1^{s^*}\right)^2\\ \phi_7 = \gamma_p + \gamma_l(n-1)\\ \phi_8 = \left(\tau_n^{v^*}\right)^2 + \gamma_p\left(\tau_{n-1}^{v^*}\right)^2 + \gamma_l\left(\tau_1^{v^*}\right)^2\end{cases} \tag{33}$$

Besides, a corresponding head-to-tail string stability crite-

rion can be derived [28, 32]:

$$\begin{aligned}Q^*_{PLF} = &-(g_n^v)^2 g_n^{\Delta v} + (g_n^v)^2 g_n^s \left(-\tfrac{1}{2}\tau_n^{v^*} - \tfrac{1}{6}\right) - g_n^v \left(g_n^{\Delta v}\right)^2 \\ &-g_n^v (g_n^s)^2 \left(\tfrac{3}{2}\left(\tau_n^{s^*}\right)^2 - 2\tau_n^{s^*}\tau_n^{v^*} + \tfrac{1}{2}\left(\tau_n^{v^*}\right)^2\right) - \tfrac{1}{2} g_n^v g_n^s \\ &-g_n^v g_n^{\Delta v} g_n^s \left(2\tau_n^{s^*} - 2\tau_n^{v^*} - \tau_n^{\Delta v^*}\right) + (g_n^v)^{-1}(g_n^s)^2 \\ &+ (S-1)\Big(-(g_n^v)^2 g_n^{\Delta v} {\phi_1}^2 + (g_n^v)^3 \phi_1 \phi_2 + (g_n^v)^2 g_n^s \phi_1 \phi_3 \\ &-g_n^v \left(g_n^{\Delta v}\right)^2 {\phi_1}^2 - g_n^v g_n^{\Delta v} g_n^s \phi_1 (2\phi_4 - \phi_5) - g_n^v g_n^s \left(\phi_7 + \tfrac{1}{2}\phi_1\right) \\ &-g_n^v (g_n^s)^2 \left({\phi_4}^2 + \tfrac{1}{2}\phi_1\phi_6 - \tfrac{1}{2}\phi_1\phi_8\right) + (g_n^v)^{-1}(g_n^s)^2\Big)\end{aligned} \tag{34}$$

For the sake of brevity of the paper, the process of deriving the head-to-tail string stability criterion is omitted. The expressions are as follows:

$$\begin{aligned}Q^*_{PF} = &-(g_n^v)^2 g_n^{\Delta v} + (g_n^v)^2 g_n^s \left(-\tfrac{1}{2}\tau_n^{v^*} - \tfrac{1}{6}\right) - g_n^v \left(g_n^{\Delta v}\right)^2 \\ &-g_n^v (g_n^s)^2 \left(\tfrac{3}{2}\left(\tau_n^{s^*}\right)^2 - 2\tau_n^{s^*}\tau_n^{v^*} + \tfrac{1}{2}\left(\tau_n^{v^*}\right)^2\right) - \tfrac{1}{2} g_n^v g_n^s \\ &-g_n^v g_n^{\Delta v} g_n^s \left(2\tau_n^{s^*} - 2\tau_n^{v^*} - \tau_n^{\Delta v^*}\right) + (g_n^v)^{-1}(g_n^s)^2 \\ &+ (S-1)\Big(-(g_n^v)^2 g_n^{\Delta v} {\varepsilon_1}^2 + (g_n^v)^3 \varepsilon_1 \gamma_p + (g_n^v)^2 g_n^s \varepsilon_1 \varepsilon_2 \\ &-g_n^v \left(g_n^{\Delta v}\right)^2 {\varepsilon_1}^2 - g_n^v g_n^{\Delta v} g_n^s \varepsilon_1 (2\varepsilon_3 - \varepsilon_4) - g_n^v g_n^s \left(\gamma_p + \tfrac{1}{2}\varepsilon_1\right) \\ &-g_n^v (g_n^s)^2 \left({\varepsilon_3}^2 + \tfrac{1}{2}\varepsilon_1\varepsilon_5 - \tfrac{1}{2}\varepsilon_1\varepsilon_6\right) + (g_n^v)^{-1}(g_n^s)^2\Big),\end{aligned} \tag{35}$$

where,

$$\begin{cases} \varepsilon_1 = 1 + \gamma_p \\ \varepsilon_2 = \left(-\tfrac{1}{2}\tau_n^{v^*} - \tfrac{1}{6}\right) + \gamma_p \left(\tfrac{1}{2}\tau_{n-1}^{v^*} - \tfrac{7}{6}\right) \\ \varepsilon_3 = \tau_n^{s^*} - \tau_n^{v^*} + \gamma_p \left(\tau_{n-1}^{s^*} - \tau_{n-1}^{v^*}\right) \\ \varepsilon_4 = \tau_n^{\Delta v^*} + \gamma_p \tau_{n-1}^{\Delta v^*} \\ \varepsilon_5 = \left(\tau_n^{s^*}\right)^2 + \gamma_p \left(\tau_{n-1}^{s^*}\right)^2 \\ \varepsilon_6 = \left(\tau_n^{v^*}\right)^2 + \gamma_p \left(\tau_{n-1}^{v^*}\right)^2. \end{cases} \tag{36}$$

$$\begin{aligned}Q^*_{MPLF} = &-(g_n^v)^2 g_n^{\Delta v} + (g_n^v)^2 g_n^s \left(-\tfrac{1}{2}\tau_n^{v^*} - \tfrac{1}{6}\right) - g_n^v \left(g_n^{\Delta v}\right)^2 \\ &-g_n^v (g_n^s)^2 \left(\tfrac{3}{2}\left(\tau_n^{s^*}\right)^2 - 2\tau_n^{s^*}\tau_n^{v^*} + \tfrac{1}{2}\left(\tau_n^{v^*}\right)^2\right) - \tfrac{1}{2} g_n^v g_n^s \\ &-g_n^v g_n^{\Delta v} g_n^s \left(2\tau_n^{s^*} - 2\tau_n^{v^*} - \tau_n^{\Delta v^*}\right) + (g_n^v)^{-1}(g_n^s)^2 \\ &+ \sum_{n=2}^{S} \Big[\Big(-(g_n^v)^2 g_n^{\Delta v} {\vartheta_1}^2 + (g_n^v)^3 \vartheta_1 \vartheta_2 + (g_n^v)^2 g_n^s \vartheta_1 \vartheta_3 \\ &-g_n^v \left(g_n^{\Delta v}\right)^2 {\vartheta_1}^2 - g_n^v g_n^{\Delta v} g_n^s \vartheta_1 (2\vartheta_4 - \vartheta_5) - g_n^v g_n^s \left(\vartheta_7 + \tfrac{1}{2}\vartheta_1\right) \\ &-g_n^v (g_n^s)^2 \left({\vartheta_4}^2 + \tfrac{1}{2}\vartheta_1\vartheta_6 - \tfrac{1}{2}\vartheta_1\vartheta_8\right) + (g_n^v)^{-1}(g_n^s)^2\Big],\end{aligned} \tag{37}$$

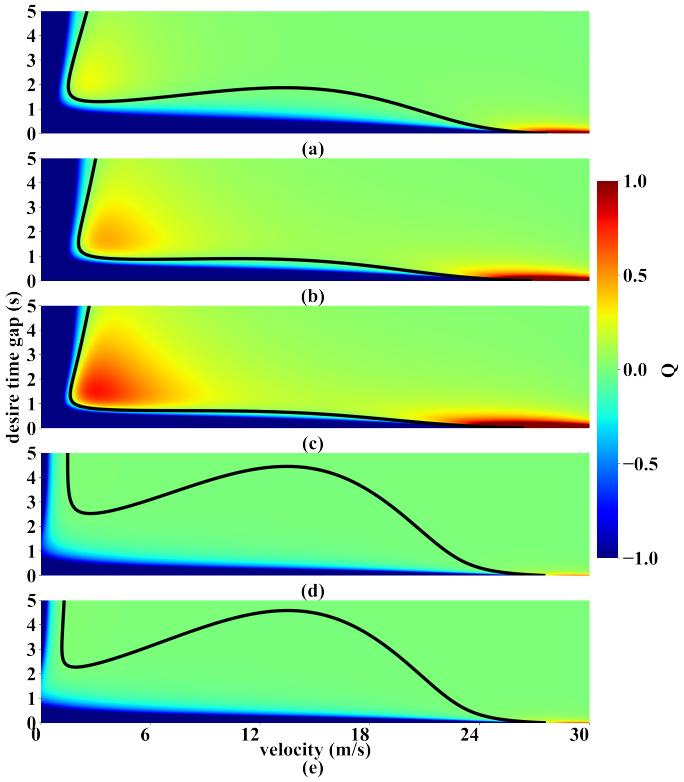

Fig. 16: The heatmaps in the velocity-desire time gap of different IFTs. (a) the case of PF; (b) the case of PLF; (c) the case of MPLF; (d) the case of ACC; (e) the case of MV.

where,

$$\begin{cases} \vartheta_1 = 1 + \sum_{k=1}^{n-1} \gamma_k \\ \vartheta_2 = \sum_{k=1}^{n-1} \frac{k(k+1)}{2}\gamma_k \\ \vartheta_3 = \left(-\tfrac{1}{2}\tau_n^{v^*} - \tfrac{1}{6}\right) + \sum_{k=1}^{n-1} \gamma_k \left(\frac{(k+1)^2 - k^2 - 2}{2}\tau_{n-\mathrm{k}}^{v^*} - \frac{(k+1)^3 - k^3}{6}\right) \\ \vartheta_4 = \tau_n^{s^*} - \tau_n^{v^*} + \sum_{k=1}^{n-1} \gamma_k \left(\tau_{n-k}^{s^*} - \tau_{n-\mathrm{k}}^{v^*}\right) \\ \vartheta_5 = \tau_n^{\Delta v^*} + \sum_{k=1}^{n-1} \gamma_k \tau_{n-k}^{\Delta v^*} \\ \vartheta_6 = \left(\tau_n^{s^*}\right)^2 + \sum_{k=1}^{n-1} \gamma_k \left(\tau_{n-k}^{s^*}\right)^2 \\ \vartheta_7 = \sum_{k=1}^{n-1} k\gamma_k \\ \vartheta_8 = \left(\tau_n^{v^*}\right)^2 + \sum_{k=1}^{n-1} \gamma_k \left(\tau_{n-k}^{v^*}\right)^2. \end{cases} \tag{38}$$

Moreover, to further explore the impact of the actuation delay on string stability, Fig. 16 shows the heatmaps in control space (velocity-desire time gap), where color represents stability margin, and the black curve in each subfigure represents the margin stable curve. When the traffic flow environment and desire time gap setting is above the margin stable curve, it is string stable at equilibrium state, while the opposite represents the unstable traffic flow.

A phenomenon can be concluded from Fig. 16 that the actuation delay deteriorates string stability, and this impact

is even worse at low velocity. No matter what kind of vehicle control strategy, string stability is not guaranteed at speed velocity, even though the desire time gap is set to 5 s. Besides, this deterioration is exacerbated as the intensity of communication increases.

VI. Conclusion

This paper designed the platoon management for CACC strings that formed several platoons due to the limitation of the C-V2X communication range. The model of CACC was firstly proposed based on specific IFTs, and multiple time delays were considered in the design of the general model. To select model parameters, corresponding linear string stability analyses were implemented to obtain the stability condition against a slight disturbance under the open boundary condition. Then, numerical analyses and simulations were carried out to verify the stability region based on the CACC platoon controller from the perspective of long-wave and short-wave stability. Finally, the differences of different IFTs in stability region, robustness, safety, and emission were explored to determine the effect of the CACC platoon controllers based on different IFTs. The following conclusions can be drawn through theoretical analysis:

1) The string stability criterion of the CACC platoon controller indicates that the linear stability is directly related to equilibrium velocity.
2) As the equilibrium velocity increases, the margin stable curve of ACC, MV, and PF will have a peak, which indicates that it is difficult for ACC to maintain stability when the equilibrium velocity is low, and the CACC platoon controller based on PLF and MPLF can directly inhibit the emergence of this peak.
3) CACC platoon controller based on IFTs can maintain a smaller desire time gap than ACC and MV without losing stability with appropriate control parameters, indicating a significant traffic capacity and safety gain via communication.
4) With the increase of the control parameters of the CACC platoon controller, the margin stable curve of the desire time gap decreases, but the decline will be smaller and smaller. Therefore, it is not necessary to set control parameters to high values. The recommended control parameter is $\gamma_p = \gamma_l = 0.3$ because the gain of the desire time gap has a diminished marginal effect with a further increase of parameters.
5) By comparing the effects of different IFTs from the four perspectives of stability, robustness, safety, and emission, we can find that PLF and MPLF can maintain a significant improvement compared to PF. Still, the difference between the two is not apparent. MPLF can keep a slight advantage in stability region, safety, and emissions, while PLF is better in robustness. However, MPLF requires an ideal communication environment that leads to exponential pressure on communication bandwidth. Its gain relative to PLF may need to be considered in a balanced manner. In general, with higher communication bandwidth or fewer communication vehicles, MPLF will be a better option; on the contrary, PLF is more suitable.

Acknowledgment

This work was sponsored by the National Science Foundation of China (No. 51878161 and No.52072067) and the China Postdoctoral Science Foundation (No.2020M681466).

Appendix

Appendix A. Platoon management strategy

Here we explain in detail why platoon management strategy is adopted and how it works.

As the standard communication protocol for CACCs selected by the Federal Communications Commission (FCC), C-V2X is significantly superior to Dedicated Short-Range Communications (DSRC) in terms of communication distance and delay. However, C-V2X is still limited by the communication bandwidth because the communication bandwidth of the C-V2X is also 20MHz same as the DSRC [44, 45, 46]. This means that the limit of channel occupancy is 20MHz, and the larger the Channel Busy Ratio (CBR), the worse the environment for communication. The impact of this limitation on the CACC platoons is that CACC platoons cannot be expanded indefinitely. Moreover, if the CBR is high, it will lead to severe Packet Error Rate (PER) and Information Age (IA), which indicates unreliable communication. As a result, all CACCs in the platoon will be forced to degrade to ACCs to avoid errors or delays in communication [47, 48].

However, according to relevant research, ACCs cannot significantly benefit traffic flow stability and capacity, while CACCs can [49, 50, 51]. Based on the above analysis, we can conclude that the benefits of CACCs can be maintained by ensuring CACCs do not degrade to ACCs as many as possible. A corresponding platoon management strategy is proposed.

According to the platoon management strategy, the first CACC beyond the maximum platoon size will automatically degrade to a leader ACC that does not accept information and only broadcasts its information. Moreover, local platoons are generated by decomposing the long platoon with the leader ACCs as the leaders of local platoons. Different local platoons apply channel scheduling methods and communicate in different channels to avoid the harsh communication environment caused by all CACCs communicating on the same channel. Based on this strategy, although the communication gain of some CACCs is sacrificed, most CACCs cannot degrade to ACCs. Thus, the benefits of CACCs on traffic flow stability and traffic capacity can be maintained under this strategy.

It is worth noting that the maximum platoon size S mentioned here can be calculated by the actual maximum C-V2X communication bandwidth and packet size. For convenience, we chose the maximum platoon size S=5 for simulation. Moreover, according to the report on the fourteenth meeting of IMT-2020 (5G) Promotion Group Cellular-Vehicle-to-everything Working Group, communication can maintain less than 47.58ms of delay, 3.12% PER, and 38.62% CBR with 54 OBUs within a 100m radius, under 10MHz channel bandwidth. This communication environment is sufficient to guarantee the platoon communicates properly under the platoon management strategy.

References

[1] Z. Wang, Y. Bian, S. E. Shladover, G. Wu, S. E. Li, and M. J. Barth, "A survey on cooperative longitudinal motion control of multiple connected and automated vehicles," *IEEE Intelligent Transportation Systems Magazine*, vol. 12, no. 1, pp. 4–24, 2019.

[2] S. E. Shladover, C. Nowakowski, X.-Y. Lu, and R. Ferlis, "Cooperative adaptive cruise control: Definitions and operating concepts," *Transportation Research Record*, vol. 2489, no. 1, pp. 145–152, 2015.

[3] J. Wang, Y. Zheng, Q. Xu, J. Wang, and K. Li, "Controllability analysis and optimal control of mixed traffic flow with human-driven and autonomous vehicles," *IEEE Transactions on Intelligent Transportation Systems*, 2020.

[4] R. Hall and C. Chin, "Vehicle sorting for platoon formation: Impacts on highway entry and throughput," *Transportation Research Part C: Emerging Technologies*, vol. 13, no. 5-6, pp. 405–420, 2005.

[5] T. Ruan, L. Zhou, and H. Wang, "Stability of heterogeneous traffic considering impacts of platoon management with multiple time delays," *Physica A: Statistical Mechanics and its Applications*, vol. 583, p. 126294, 2021.

[6] Y. Qin, H. Wang, and D. Ni, "Lighthill-whitham-richards model for traffic flow mixed with cooperative adaptive cruise control vehicles," *Transportation Science*, vol. 55, no. 4, pp. 883–907, 2021.

[7] L. Zhou, T. Ruan, K. Ma, C. Dong, and H. Wang, "Impact of cav platoon management on traffic flow considering degradation of control mode," *Physica A: Statistical Mechanics and its Applications*, p. 126193, 2021.

[8] Y. Zhang, Y. Bai, J. Hu, and M. Wang, "Control design, stability analysis, and traffic flow implications for cooperative adaptive cruise control systems with compensation of communication delay," *Transportation Research Record*, vol. 2674, no. 8, pp. 638–652, 2020.

[9] F. Navas and V. Milanés, "Mixing v2v-and non-v2v-equipped vehicles in car following," *Transportation research part C: emerging technologies*, vol. 108, pp. 167–181, 2019.

[10] C. Wang, S. Gong, A. Zhou, T. Li, and S. Peeta, "Cooperative adaptive cruise control for connected autonomous vehicles by factoring communication-related constraints," *Transportation Research Part C: Emerging Technologies*, vol. 113, pp. 124–145, 2020.

[11] K. Li, Y. Bian, S. E. Li, B. Xu, and J. Wang, "Distributed model predictive control of multi-vehicle systems with switching communication topologies," *Transportation Research Part C: Emerging Technologies*, vol. 118, p. 102717, 2020.

[12] A. Zhou, S. Gong, C. Wang, and S. Peeta, "Smooth-switching control-based cooperative adaptive cruise control by considering dynamic information flow topology," *Transportation Research Record*, vol. 2674, no. 4, pp. 444–458, 2020.

[13] Y. Zheng, S. E. Li, J. Wang, D. Cao, and K. Li, "Stability and scalability of homogeneous vehicular platoon: Study on the influence of information flow topologies," *IEEE Transactions on intelligent transportation systems*, vol. 17, no. 1, pp. 14–26, 2015.

[14] Y. Zheng, S. E. Li, K. Li, and W. Ren, "Platooning of connected vehicles with undirected topologies: Robustness analysis and distributed h-infinity controller synthesis," *IEEE Transactions on Intelligent Transportation Systems*, vol. 19, no. 5, pp. 1353–1364, 2017.

[15] Y. Bian, Y. Zheng, W. Ren, S. E. Li, J. Wang, and K. Li, "Reducing time headway for platooning of connected vehicles via v2v communication," *Transportation Research Part C: Emerging Technologies*, vol. 102, pp. 87–105, 2019.

[16] H. Liu, X. D. Kan, S. E. Shladover, X.-Y. Lu, and R. E. Ferlis, "Modeling impacts of cooperative adaptive cruise control on mixed traffic flow in multi-lane freeway facilities," *Transportation Research Part C: Emerging Technologies*, vol. 95, pp. 261–279, 2018.

[17] Z. Yang, Y. Feng, and H. X. Liu, "A cooperative driving framework for urban arterials in mixed traffic conditions," *Transportation research part C: emerging technologies*, vol. 124, p. 102918, 2021.

[18] D. Jia, K. Lu, J. Wang, X. Zhang, and X. Shen, "A survey on platoon-based vehicular cyber-physical systems," *IEEE communications surveys & tutorials*, vol. 18, no. 1, pp. 263–284, 2015.

[19] F. Ma, J. Wang, Y. Yang, L. Wu, S. Zhu, S. Y. Gelbal, B. Aksun-Guvenc, and L. Guvenc, "Stability design for the homogeneous platoon with communication time delay," *Automotive Innovation*, vol. 3, pp. 101–110, 2020.

[20] Y. Zheng, S. E. Li, J. Wang, K. Li *et al.*, "Influence of information flow topology on closed-loop stability of vehicle platoon with rigid formation," in *17th International IEEE Conference on Intelligent Transportation Systems (ITSC)*. IEEE, 2014, pp. 2094–2100.

[21] H. Farah and H. N. Koutsopoulos, "Do cooperative systems make drivers' car-following behavior safer?" *Transportation research part C: emerging technologies*, vol. 41, pp. 61–72, 2014.

[22] S. Yu and Z. Shi, "The effects of vehicular gap changes with memory on traffic flow in cooperative adaptive cruise control strategy," *Physica A: Statistical Mechanics and its Applications*, vol. 428, pp. 206–223, 2015.

[23] Z. Li, W. Li, S. Xu, and Y. Qian, "Stability analysis of an extended intelligent driver model and its simulations under open boundary condition," *Physica A: Statistical Mechanics and its Applications*, vol. 419, pp. 526–536, 2015.

[24] P. Fernandes and U. Nunes, "Multiplatooning leaders positioning and cooperative behavior algorithms of communicant automated vehicles for high traffic capacity," *IEEE Transactions on Intelligent Transportation Systems*, vol. 16, no. 3, pp. 1172–1187, 2014.

[25] V. Milanés and S. E. Shladover, "Modeling cooperative and autonomous adaptive cruise control dynamic responses using experimental data," *Transportation Research Part C: Emerging Technologies*, vol. 48, pp. 285–

300, 2014.

[26] V. Milanés, S. E. Shladover, J. Spring, C. Nowakowski, H. Kawazoe, and M. Nakamura, "Cooperative adaptive cruise control in real traffic situations," *IEEE Transactions on intelligent transportation systems*, vol. 15, no. 1, pp. 296–305, 2013.

[27] K. C. Dey, L. Yan, X. Wang, Y. Wang, H. Shen, M. Chowdhury, L. Yu, C. Qiu, and V. Soundararaj, "A review of communication, driver characteristics, and controls aspects of cooperative adaptive cruise control (cacc)," *IEEE Transactions on Intelligent Transportation Systems*, vol. 17, no. 2, pp. 491–509, 2015.

[28] D. Ngoduy, "Analytical studies on the instabilities of heterogeneous intelligent traffic flow," *Communications in Nonlinear Science and Numerical Simulation*, vol. 18, no. 10, pp. 2699–2706, 2013.

[29] Z. Yao, T. Xu, Y. Jiang, and R. Hu, "Linear stability analysis of heterogeneous traffic flow considering degradations of connected automated vehicles and reaction time," *Physica A: Statistical Mechanics and its Applications*, vol. 561, p. 125218, 2021.

[30] I. G. Jin and G. Orosz, "Dynamics of connected vehicle systems with delayed acceleration feedback," *Transportation Research Part C: Emerging Technologies*, vol. 46, pp. 46–64, 2014.

[31] J. Sun, Z. Zheng, and J. Sun, "Stability analysis methods and their applicability to car-following models in conventional and connected environments," *Transportation research part B: methodological*, vol. 109, pp. 212–237, 2018.

[32] J. A. Ward, "Heterogeneity, lane-changing and instability in traffic : A mathematical approach," *University of Bristol*, 2009.

[33] X. Chang, H. Li, J. Rong, X. Zhao *et al.*, "Analysis on traffic stability and capacity for mixed traffic flow with platoons of intelligent connected vehicles," *Physica A: Statistical Mechanics and its Applications*, vol. 557, p. 124829, 2020.

[34] Y. Li, H. Wang, W. Wang, L. Xing, S. Liu, and X. Wei, "Evaluation of the impacts of cooperative adaptive cruise control on reducing rear-end collision risks on freeways," *Accident Analysis & Prevention*, vol. 98, pp. 87–95, 2017.

[35] A. Kesting, M. Treiber, M. Schönhof, and D. Helbing, "Adaptive cruise control design for active congestion avoidance," *Transportation Research Part C: Emerging Technologies*, vol. 16, no. 6, pp. 668–683, 2008.

[36] A. Kesting, M. Treiber, M. Schönhof, F. Kranke, and D. Helbing, "Jam-avoiding adaptive cruise control (acc) and its impact on traffic dynamics," in *Traffic and Granular Flow'05*. Springer, 2007, pp. 633–643.

[37] S. Gong, J. Shen, and L. Du, "Constrained optimization and distributed computation based car following control of a connected and autonomous vehicle platoon," *Transportation Research Part B: Methodological*, vol. 94, pp. 314–334, 2016.

[38] X. Li, J. Cui, S. An, and M. Parsafard, "Stop-and-go traffic analysis: Theoretical properties, environmental impacts and oscillation mitigation," *Transportation Research Part B: Methodological*, vol. 70, pp. 319–339, 2014.

[39] K. A. Hafeez, L. Zhao, B. Ma, and J. W. Mark, "Performance analysis and enhancement of the dsrc for vanet's safety applications," *IEEE Transactions on Vehicular Technology*, vol. 62, no. 7, pp. 3069–3083, 2013.

[40] L. I. Panis, S. Broekx, and R. Liu, "Modelling instantaneous traffic emission and the influence of traffic speed limits," *Science of the total environment*, vol. 371, no. 1-3, pp. 270–285, 2006.

[41] L. Xiao, S. Darbha, and F. Gao, "Stability of string of adaptive cruise control vehicles with parasitic delays and lags," in *IEEE Conference on Intelligent Transportation Systems, Proceedings, ITSC*. IEEE, 2008, pp. 1101–1106.

[42] L. Xiao and F. Gao, "Practical string stability of platoon of adaptive cruise control vehicles," *IEEE Transactions on intelligent transportation systems*, vol. 12, no. 4, pp. 1184–1194, 2011.

[43] M. Wang, S. P. Hoogendoorn, W. Daamen, B. van Arem, B. Shyrokau, and R. Happee, "Delay-compensating strategy to enhance string stability of adaptive cruise controlled vehicles," *Transportmetrica B: Transport Dynamics*, vol. 6, no. 3, pp. 211–229, 2018.

[44] A. Boubakri and S. M. Gammar, "Intra-platoon communication in autonomous vehicle: A survey," in *2020 9th IFIP International Conference on Performance Evaluation and Modeling in Wireless Networks (PEMWN)*. IEEE, 2020, pp. 1–6.

[45] S. Chen, J. Hu, Y. Shi, L. Zhao, and W. Li, "A vision of C-V2X: Technologies, field testing, and challenges with chinese development," *IEEE Internet of Things Journal*, vol. 7, no. 5, pp. 3872–3881, 2020.

[46] G. Nardini, A. Virdis, C. Campolo, A. Molinaro, and G. Stea, "Cellular-V2X communications for platooning: Design and evaluation," *Sensors*, vol. 18, no. 5, p. 1527, 2018.

[47] V. Vukadinovic, K. Bakowski, P. Marsch, I. D. Garcia, H. Xu, M. Sybis, P. Sroka, K. Wesolowski, D. Lister, and I. Thibault, "3GPP C-V2X and IEEE 802.11 p for Vehicle-to-Vehicle communications in highway platooning scenarios," *Ad Hoc Networks*, vol. 74, pp. 17–29, 2018.

[48] H. V. Vu, Z. Liu, D. H. N. Nguyen, R. Morawski, and T. Le-Ngoc, "Multi-agent reinforcement learning for joint channel assignment and power allocation in platoon-based C-V2X systems," *arXiv preprint arXiv:2011.04555*, 2020.

[49] M. Shang and R. E. Stern, "Impacts of commercially available adaptive cruise control vehicles on highway stability and throughput," *Transportation Research Part C: Emerging Technologies*, vol. 122, p. 102897, 2021.

[50] S. E. Shladover, D. Su, and X.-Y. Lu, "Impacts of cooperative adaptive cruise control on freeway traffic flow," *Transportation Research Record*, vol. 2324, no. 1, pp. 63–70, 2012.

[51] I. K. Nikolos, A. I. Delis, and M. Papageorgiou, "Macro-

scopic modelling and simulation of ACC and CACC traffic," in *2015 IEEE 18th International Conference on Intelligent Transportation Systems*. IEEE, 2015, pp. 2129–2134.

PLACE PHOTO HERE

Tiancheng Ruan Tiancheng Ruan received the B.Eng. degrees in transportation planning and management from Chang'an University, Xi'an, China, in 2019. He is currently pursuing the Ph.D. degree with School of Transportation in Southeast University. His research interests include traffic flow theory, intelligent transportation systems, and stability analyses.

PLACE PHOTO HERE

Hao Wang Tiancheng Ruan received the B.Eng. degrees in transportation planning and management from Chang'an University, Xi'an, China, in 2019. He is currently pursuing the Ph.D. degree with School of Transportation in Southeast University. His research interests include traffic flow theory, intelligent transportation systems, and stability analyses.

PLACE PHOTO HERE

Linjie Zhou Tiancheng Ruan received the B.Eng. degrees in transportation planning and management from Chang'an University, Xi'an, China, in 2019. He is currently pursuing the Ph.D. degree with School of Transportation in Southeast University. His research interests include traffic flow theory, intelligent transportation systems, and stability analyses.

PLACE PHOTO HERE

Yantang Zhang Tiancheng Ruan received the B.Eng. degrees in transportation planning and management from Chang'an University, Xi'an, China, in 2019. He is currently pursuing the Ph.D. degree with School of Transportation in Southeast University. His research interests include traffic flow theory, intelligent transportation systems, and stability analyses.

PLACE PHOTO HERE

Changyin Dong Tiancheng Ruan received the B.Eng. degrees in transportation planning and management from Chang'an University, Xi'an, China, in 2019. He is currently pursuing the Ph.D. degree with School of Transportation in Southeast University. His research interests include traffic flow theory, intelligent transportation systems, and stability analyses.

PLACE PHOTO HERE

Zewen Zuo Tiancheng Ruan received the B.Eng. degrees in transportation planning and management from Chang'an University, Xi'an, China, in 2019. He is currently pursuing the Ph.D. degree with School of Transportation in Southeast University. His research interests include traffic flow theory, intelligent transportation systems, and stability analyses.